Gaia Data Release 2

Astronomy & Astrophysics manuscript no. GAIA-DR2-CU6VR-DK
December 5, 2018

Gaia Data Release 2
Properties and validation of the radial velocities

D. Katz[1], P. Sartoretti[1], M. Cropper[2], P. Panuzzo[1], G.M. Seabroke[2], Y. Viala[1], K. Benson[2], R. Blomme[3], G. Jasniewicz[4], A. Jean-Antoine[5], H. Huckle[2], M. Smith[2], S. Baker[2], F. Crifo[1], Y. Damerdji[6,7], M. David[8], C. Dolding[2], Y. Frémat[3], E. Gosset[7,9], A. Guerrier[10], L.P. Guy[11], R. Haigron[1], K. Janßen[12], O. Marchal[1], G. Plum[1], C. Soubiran[13], F. Thévenin[14], M. Ajaj[1], C. Allende Prieto[2,15,16], C. Babusiaux[1,17], S. Boudreault[2,18], L. Chemin[13,19], C. Delle Luche[1,10], C. Fabre[20], A. Gueguen[1,21], N.C. Hambly[22], Y. Lasne[5], F. Meynadier[1,23], F. Pailler[5], C. Panem[5], F. Royer[1], G. Tauran[5], C. Zurbach[4], T. Zwitter[24], F. Arenou[1], D. Bossini[25], J. Gerssen[12], A. Gómez[1], V. Lemaitre[5], N. Leclerc[1], T. Morel[7], U. Munari[26], C. Turon[1], A. Vallenari[25], and M. Žerjal[24,27]

(Affiliations can be found after the references)

Received **Month Day, 201X**; accepted **Month Day, 201X**

ABSTRACT

Context. For *Gaia* DR2, 280 million spectra, collected by the *Radial Velocity Spectrometer* instrument on-board *Gaia*, were processed and median radial velocities were derived for 9.8 million sources brighter than $G_{\rm RVS} = 12$ mag.

Aims. This paper describes the validation and properties of the median radial velocities published in *Gaia* DR2.

Methods. Quality tests and filters are applied to select, from the 9.8 million radial velocities, those with the quality to be published in *Gaia* DR2. The accuracy of the selected sample is assessed with respect to ground-based catalogues. Its precision is estimated using both ground-based catalogues and the distribution of the *Gaia* radial velocity uncertainties.

Results. *Gaia* DR2 contains median radial velocities for 7 224 631 stars, with $T_{\rm eff}$ in the range $[3550, 6900]$ K, which passed succesfully the quality tests. The published median radial velocities provide a full sky-coverage and have a completness with respect to the astrometric data of 77.2% (for $G \leq 12.5$ mag). The median radial velocity residuals with respect to the ground-based surveys vary from one catalogue to another, but do not exceed a few 100s m s^{-1}. In addition, the *Gaia* radial velocities show a positive trend as a function of magnitude, which starts around $G_{\rm RVS} \sim 9$ mag and reaches about +500 m s^{-1} at $G_{\rm RVS} = 11.75$ mag. The origin of the trend is under investigation, with the aim to correct for it in *Gaia* DR3. The overall precision, estimated from the median of the *Gaia* radial velocity uncertainties, is 1.05 km s^{-1}. The radial velocity precision is function of many parameters, in particular the magnitude and effective temperature. For bright stars, $G_{\rm RVS} \in [4, 8]$ mag, the precision, estimated using the full dataset, is in the range 220-350 m s^{-1}, which is about 3 to 5 times more precise than the pre-launch specification of 1 km s^{-1}. At the faint end, $G_{\rm RVS} = 11.75$ mag, the precisions for $T_{\rm eff} = 5000$ K and 6500 K are respectively 1.4 km s^{-1} and 3.7 km s^{-1}.

Key words. Techniques: spectroscopic; Techniques: radial velocities; Catalogues; Surveys;

1. Introduction

ESA's *Gaia* mission (Gaia Collaboration et al. 2016b) was launched from the Kourou space centre on 19th December 2013. It took about 4 weeks to the satellite to reach its operational orbit around the second Lagrange point (L2) of the Sun-Earth system. Following the commissioning phase, the nominal mission began on 25th July 2014, initially for a 5 year period, which has recently been granted a first extension by 1.5 years[1]. *Gaia* scans continuously the celestial sphere with its 2 telescopes and its 3 instruments: the astrometric instrument, a spectro-photometer and a medium resolving power spectrograph, the *Radial Velocity Spectrometer* (RVS, Cropper et al. 2018). The data collected are transmitted daily to Earth, when the satellite is in contact with one of the ground-based antennae. Once received on the ground, the data are processed by the *Gaia Data Processing and Analysis Consortium* (DPAC). The consortium publishes the products of the processing in successive data releases. The first one, *Gaia* DR1 (Gaia Collaboration et al. 2016a) was issued on 16th September 2016 and the second one, *Gaia* DR2 (Gaia Collaboration et al. 2018b), on 25th April 2018.

[1] The current cold gas fuel supplies of *Gaia* would allow to extend the nominal mission by 5 years.

Each new *Gaia* data release comes with new products. One of the novelties of *Gaia* DR2 is the publication of the median radial velocities, extracted from the RVS spectra. The *Radial Velocity Spectrometer* collects spectra down to $G_{\rm RVS} = 16.2$ mag. Yet, because of the modest exposure time per CCD of 4.42 s, the signal-to-noise ratio of the spectra of the faintest stars is very low. The derivation of the radial velocities of the faintest stars will require to combine all the spectroscopic information collected for each source over the full mission. For *Gaia* DR2, 280 million spectra, recorded during the 22 first months of the nominal mission, were processed and median radial velocities were obtained for 9.8 million stars down to magnitude $G_{\rm RVS} = 12$ mag. The spectroscopic pipeline and the processing of the spectra are described in details in a companion paper (Sartoretti et al. 2018).

During the last 15 years, spectroscopic surveys have delivered radial velocities, as well as stellar parameters and abundances, for large stellar samples, e.g. Geneva-Copenhagen-Survey (Nordström et al. 2004): ∼17 000 stars, SEGUE (Yanny et al. 2009): ∼240 000 stars, APOGEE (Holtzman et al. 2015): ∼150 000 stars, APOGEE-2 (Majewski et al. 2017; Abolfathi et al. 2017): ∼263 000 stars, RAVE (Steinmetz et al. 2006; Kunder et al. 2017): ∼460 000 stars **in DR5**, Gaia-ESO-Survey

(Gilmore et al. 2012; Sacco et al. 2014; Jackson et al. 2015): ~50 000 stars in DR3, LAMOST (Cui et al. 2012; Zhao et al. 2012): ~5.3 million stars in DR5, **GALAH** (Buder et al. 2018; Zwitter et al. 2018): ~340 000 stars in DR2. In the continuity of these large surveys, *Gaia* DR2 contains median radial velocities for 7 224 631 stars with $T_{\rm eff}$ in the range [3550, 6900] K and distributed over the full celestial sphere.

This paper is devoted to the description and validation of the median radial velocities published in *Gaia* DR2. After a short summary of the main characteristics of the *Radial Velocity Spectrometer* instrument (Sect. 2) and a brief overview of the spectroscopic processing pipeline (Sect. 3), Sect. 4 presents the filters that were applied after the completion of the processing, to select the radial velocities with the quality to be published in *Gaia* DR2. Sect. 5 describes the properties of the published radial velocities.

2. The Radial Velocity Spectrometer

The *Radial Velocity Spectrometer* (RVS) is described in details in (Cropper et al. 2018). Here we provide a very brief description of the main characteristics of the instrument.

The *Radial Velocity Spectrometer* is a medium resolving power, $R = \lambda/\Delta\lambda = 11\,500$, near-infrared $\lambda \in [845, 872]$ nm, integral field spectrograph. As the astrometric and photometric instruments, the RVS is illuminated by the two Gaia telescopes. The spectra are recorded on a block of 12 CCDs (3 in the direction of the scan times 4 in the direction perpendicular to the scan) located at the edge of the Gaia focal plane. When a source crosses one of the two fields of view (hereafter referred to as *transit*), 3 spectra are recorded, i.e. one per CCD along the scan direction. The exposure time per CCD is 4.42 s. On average, the RVS should record 40 transits per source during the 5 years of the nominal mission.

Gaia is continuously spinning and scanning the sky with a 6 hour period. The CCDs are therefore operated in *Time Delay Integration* (TDI) mode, i.e. the charges are transferred from columns to columns at high frequency, in order to follow the sources during their crossing of the focal plane. In order to minimize both the telemetry budget and the electronic noise, elongated windows are read around the spectra and transmitted to the ground. The rest of the pixels are flushed in the readout register and discarded. At the start of the nominal mission, the windows were 1260 pixels long (i.e. in the sense of the spectral dispersion which is also the orientation of the scan) and 10 pixels wide. The length of the windows was increased to 1296 pixels in Spring 2015 to allow for a better measure of the background light. The on-board software allocates windows to sources down to $G_{\rm RVS}$= 16.2 mag, which is the limiting magnitude of the RVS.

The RVS is an integral field spectrograph and, as such, disperses the light of all the sources contained in its two fields of view, with the consequence that the spectra of very close neighbours will overlap. In this case, to avoid transmitting twice the pixels, the on-board software can decide to truncate the windows in the direction perpendicular to the dispersion, i.e. allocating less than 10 pixels to the window width. If the conflict does not extend on the full length of the spectrum, the truncation will be applied only to the appropriate portion of the spectrum, resulting in a non-rectangular window. For *Gaia* DR2, only rectangular windows were processed. The specific treatments required by non rectangular windows are planned for *Gaia* DR3.

During commissioning, it was found that the level of stray light was higher than expected. Although the spectroscopic pipeline subtracts the scattered light, the noise in the spectra is increased. This affects more strongly the faint stars, in particular those *close* to the RVS limiting magnitude. The origin, properties, on-board mitigation and consequences of the stray light are described in Cropper et al. (2018). The treatment of the scattered light by the spectroscopic pipeline is presented in Sartoretti et al. (2018).

In *Gaia* DR2, median radial velocities are published for stars with $T_{\rm eff}$ in the interval [3550, 6900] K. In this temperature range, the RVS spectra are dominated by a triplet of the ionised calcium. The wavelength range also contains weaker neutral metallic lines of, e.g. iron, silicon or titanium. As an example, Fig. 1 presents the RVS spectrum of the star HIP 58558: $T_{\rm eff}$ = 5477 K, $\log g$ = 4.34 and [Fe/H] = 0.02 dex (Adibekyan et al. 2012). Below about 3400 K, the RVS spectra develop strong molecular bands. In A and B spectral types, the P13 to P17 hydrogen Paschen lines become the dominant spectral features. As discussed in Sect. 4, the radial velocities of *cool* and *hot* stars, i.e. outside [3550, 6900] K, will be published in a future *Gaia* release.

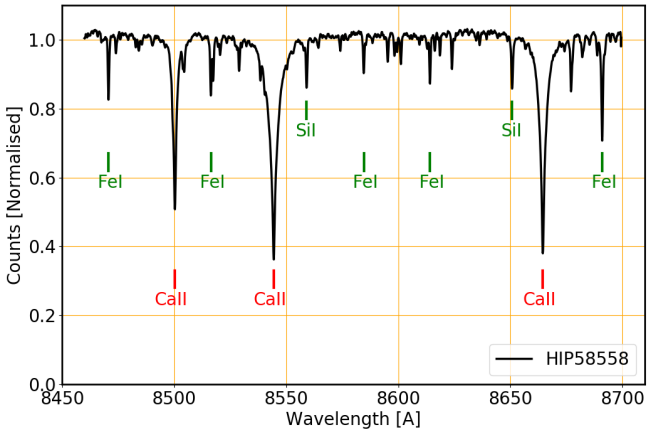

Fig. 1: RVS spectrum of the star HIP 58558.

3. The spectroscopic pipeline

3.1. Overview

The *Gaia* spectroscopic processing pipeline is described in details in Sartoretti et al. (2018). In this section, we provide a brief overview of its functionalities.

The spectroscopic pipeline is in charge of four main tasks:

1. *Calibrating the RVS instrument.* The pipeline developed for *Gaia* DR2 calibrates: the electronic bias, the read-out noise, the wavelengths and the $G_{\rm RVS}$ magnitude zero-point. For the other RVS characteristics, the pipeline relies either on pre-launch or off-line calibrations.
2. *Reducing and cleaning the spectra.* This includes in particular, e.g. subtracting the electronic bias and the straylight, discarding spectra degraded by CCD cosmetic defects or saturation, applying the wavelength calibration, removing the cosmic rays, normalising the continuum, deriving the internal $G_{\rm RVS}$ magnitude, selecting a template to derive the radial velocity.

3. *Measuring the radial velocities per transit.* For each star and for each transit one (or two, in the case of a double star) radial velocity is measured. Each radial velocity is derived by a series of modules which compare the 3 RVS spectra collected per transit to one (or several) template(s) shifted step by step in radial velocity, from −1000 to +1000 km s^{-1}. This workflow is hereafter referred to as *Single Transit Analysis (STA)*.
4. *Combining the information of the successive transits.* For each source, the radial velocities derived on successive transits are grouped in a time series. The radial velocities published in *Gaia* DR2 are the medians of these time series (see Sect. 5.1.1 for more details). Statistical properties of the time series are also calculated and are used as variability and quality indicators. In addition, for each source, all the spectra recorded are shifted to rest frame and combined. The combined spectra are then examined in order to detect possible emission lines. This set of tasks is hereafter referred to as *Multiple Transit Analysis (MTA)*.

3.2. Selection of the templates

The proper selection of the templates and their similarities with the observed spectra play an important role in the quality of the radial velocities derived (see Sect. 4 and 5). Because of its impact on the performance, we present here this specific task of the pipeline. A more detailed description is provided in Sartoretti et al. (2018).

About 15% of the stars processed for *Gaia* DR2 had known ground-based atmospheric parameters. When available, this information was used to select the closest template in a library of several thousands synthetic spectra. When the parameters were unknown, a dedicated software module, *determineAP*, was in charge of choosing the template by comparison of the RVS spectrum to a set a synthetic spectra. For *Gaia* DR2, 280 million spectra were processed. The volume of data was too large to compare 85% of the RVS spectra to the full library of synthetic spectra. To keep the processing load reasonable, *determineAP* had to select the templates in a sub-grid restricted to 28 synthetic spectra. The sub-grid contains 18 different temperatures, ranging from 3 100 to 35 000 K, 2 metallicities: solar for all the temperatures and [Fe/H]= −1.5 dex for 9 of them and a single choice of surface gravity for most temperatures. In STA, a single template is used per star, i.e. the same for all the transits.

3.3. The $G_{\rm RVS}$ and G magnitudes

Different measures of the $G_{\rm RVS}$ magnitude are either produced or used by the pipeline and in this paper. They are defined below:

- The *On-board* $G_{\rm RVS}$ ($G_{\rm RVS}^{\rm on-board}$) is derived by the Gaia on-board software.
- The *External* $G_{\rm RVS}$ ($G_{\rm RVS}^{\rm ext}$) is calculated from ground-based photometric catalogues using colour-colour transformations. When no ground-based photometry is available, the on-board $G_{\rm RVS}^{\rm on-board}$ is adopted. $G_{\rm RVS}^{\rm ext}$ is the magnitude used to define the limiting magnitude of *Gaia* DR2: $G_{\rm RVS}^{\rm ext} \leq 12$ mag.
- The *Internal* $G_{\rm RVS}$ ($G_{\rm RVS}^{\rm int}$) is measured by the spectroscopic pipeline (Sartoretti et al. 2018) from the RVS spectra. For the faint stars, the accuracy and precision of $G_{\rm RVS}^{\rm int}$ are limited by the basic modelling of the straylight in *Gaia* DR2. A more elaborated calibration of the straylight is in development for *Gaia* DR3.

In Sect. 5.1, the completeness is assessed as a function of the G magnitude, which is the *Gaia* broad band magnitude measured from the astrometric windows (Riello et al. 2018; Evans et al. 2018). The colour of a typical un-reddened G2V star is $G - G_{\rm RVS} \sim 0.65$ mag (Jordi et al. 2010).

4. Selecting radial velocities for publication in *Gaia* DR2

For *Gaia* DR2, the spectroscopic pipeline has processed 280 million spectra and produced radial velocities for 9.8 million stars without pre-selection on spectral type or colour indices and for a very broad range of signal to noise ratios. The pipeline includes validation functionalities, described in Sartoretti et al. (2018), which can autonomously identify and reject problematic data: e.g. negative total spectrum flux or nearby duplicated transits. These diagnostics are usually meant to detect issues at spectrum or transit level. They do not consider the global properties of the data (known a posteriori) and the potential outliers. Therefore, following the completion of the processing, an off-line validation campaign was conducted on the full 9.8 million stars sample to assess its characteristics and identify the stars which did not have the quality to be published in *Gaia* DR2. This resulted in the following list of filters:

Large coordinate uncertainties. The right ascensions and declinations (computed by the *Gaia* astrometric pipeline, see Lindegren et al. 2018) are used to derive the coordinates of the sources in the RVS fields of view, which are then used to calibrate the spectra in wavelength. The uncertainties on the coordinates of the sources are therefore propagated to the wavelengths of the spectra and *in fine* to the radial velocities. In *Gaia* DR2, the mean precision on the source positions is 0.03 mas, which represents a very minor contribution to the radial velocity error budget of ~ 4.3 m s^{-1}. Of course, a small fraction of the stars presents much larger astrometric uncertainties. The radial velocities of ∼8 000 stars with a quadratic sum of the uncertainties on the right ascension and on the declination, i.e. $\sqrt{\epsilon_\alpha^2 + \epsilon_\delta^2}$, larger than 100 mas (corresponding to $\sim$ 14.5 km/s) were discarded from *Gaia* DR2.

Faint stars. For *Gaia* DR2, stars brighter than $G_{\rm RVS}^{\rm ext} = 12$ mag were processed by the spectroscopic pipeline. The selection was performed using the external $G_{\rm RVS}^{\rm ext}$ magnitude (see Sect. 3.3). The spectroscopic pipeline also derives an internal $G_{\rm RVS}^{\rm int}$ magnitude based on the flux contained in the RVS spectrum between 846 and 870 nm. It was considered that the ∼165 000 stars with an internal $G_{\rm RVS}^{\rm int}$ magnitude equal to or fainter than 14 mag were not containing enough signal per spectrum to yield a good enough velocity in *Gaia* DR2.

Ambiguous transits. The *Single Transit Analysis (STA)* workflow produces a boolean quality flag, *isAmbiguous*[2], which identifies the radial velocities which look suspicious on a specific transit. In validation, the ratio of the number of *ambiguous* transits over the total number transits, for each source, was examined. The distribution on the celestial sphere

[2] A radial velocity derivation module will flag a transit radial velocity as *isAmbiguous* if two or more of the three velocities derived for the three RVS CCDs (crossed during that transit) are too discrepant. A detailed description of the derivation of the *isAmbiguous* flag is provided in Sect. 7.7 of Sartoretti et al. (2018).

of this new quality indicator shows a very specific pattern. While on most of the sky, the mode of its distribution peaks at 0, in a few specific areas it peaks at 1 (i.e. peaks at 100% of ambiguous transits per source). This behaviour seems, for a part, related to the overestimation of the external $G_{\rm RVS}^{\rm ext}$ magnitude in some specific areas, allowing some faint stars to enter the spectroscopic processing. The radial velocities of the ∼611 000 stars with 100% ambiguous transits were excluded from *Gaia* DR2. The two filters on *faint stars* and *ambiguous transits* show some overlap, both rejecting stars with too low signal in the RVS window. Yet, because they consider different quantities, they are also complementary, one possibly identifying a suspicious star that the other could have missed.

Large radial velocity uncertainties. The distribution of unfiltered radial velocity uncertainties peaks between 1 and 2 km/s and shows either an extended tail or a broad small amplitude secondary peak (depending on the location on the sky). The extended tail/secondary peak includes a mix of stars with insufficient signal to be processed in *Gaia* DR2, large amplitude variables and undetected binary or multiple systems. In all these cases, the median radial velocity published in *Gaia* DR2 would not be a reliable estimate of the source or system radial velocity. The median radial velocities of the ∼1.6 million stars with a radial velocity uncertainty larger or equal to 20 km/s were discarded from *Gaia* DR2.

Suspected double line spectroscopic binaries. The *Single Transit Analysis* workflow includes a software module which is in charge of detecting the spectra presenting double line patterns and to derive their two radial velocities. The multi-instrument modelling and publication of binary systems is planned for *Gaia* DR3. Therefore, in *Gaia* DR2, the ∼113 000 stars with more than 10% of their transits flagged as double-line patterns were considered as potential double-lines spectroscopic binaries (SB2) and their median radial velocities were removed from *Gaia* DR2.

Suspected emission line stars. The *Multiple Transit Analysis (MTA)* workflow includes a software module in charge of detecting emission line stars. The library of spectra used for *Gaia* DR2 does not contain emission line templates. The comparison of an emission line star with an inappropriate absorption line template can produce systematic radial velocity shifts of several hundreds km s^{-1}. The radial velocities of ∼7 000 stars identified as potential emission line ones were excluded from *Gaia* DR2. Figure 2 shows, as an example, the RVS spectrum of the star HIP 55044, which has been detected as an emission line star by the *MTA* workflow. It is classified in the literature as a Be star (Houk & Cowley 1975).

Cool stars. In the RVS domain, the spectra of late M-stars are dominated by TiO molecular bands. The spectra show steep slopes and because of the narrow RVS wavelength range, the pseudo-continuum is usually not visible on the side of the shortest wavelengths. For these stars, the radial velocity precision is more sensitive, than for other spectral types, to the treatment of the continuum as well as to the choice of the template. Tests conducted during the validation phase showed that the radial velocity performance were significantly lower for the stars processed using templates with effective temperatures of 3500 K or lower. The radial velocities of ∼747 000 stars processed with a *cold-star* template were removed from *Gaia* DR2. The spectroscopic pipeline will be upgraded to process late M-type stars and publish their radial velocities in a future *Gaia* data release.

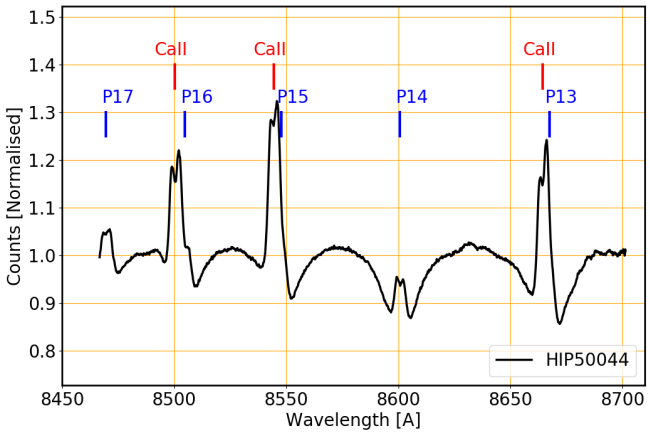

Fig. 2: RVS spectrum of the Be star HIP 55044. Both the Ca II and the Paschen lines are in emission.

Hot stars. The validation phase showed that the 28 synthetic spectra available to the module *determineAP* to select the templates (see Sect. 3.2), and in particular the single choice of gravity per effective temperature, were insufficient for hot stars. In early F and A-type stars, the Paschen lines are significantly pressure sensitive and get stronger with decreasing surface gravity. Three of the Paschen lines, i.e. P13, P15 and P16, are blended with the Ca II lines. The profiles of the blended lines change with surface gravity and as a consequence, the centroids of the lines are shifted. This can produce a systematic bias on the radial velocity of several km s^{-1}, if it is derived with the inappropriate template. The systematic error can be amplified if the star shows a significant projected rotational velocity, which will modify more the "narrow" profile of the Ca II lines than the broader profiles of the Paschen lines. Therefore, the ∼996 000 radial velocities derived using a template with an effective temperature of 7 000 K or higher were excluded from *Gaia* DR2.

Figure 3 illustrates the sensitivity of the Ca II-Paschen blends to surface gravity and rotational velocity. HIP 66525 (top) has a $T_{\rm eff}$ ∼ 8000 K and a $\log g$ ∼ 4.6 (Kordopatis et al. 2013), while HIP 91843 (bottom) has a $T_{\rm eff}$ ∼ 8100 K and a $\log g$ ∼ 3.2 (derived from 2MASS photometry). One can see that the Paschen lines are stronger in the latter than in the former. Moreover, in HIP 91843, the depth of the Ca II lines is reduced by the projected rotational velocity broadening.

In *Gaia* DR3 and following releases, the atmospheric parameters should be derived by elaborated analysis of the *Gaia* spectro-photometric data and, for the brightest stars, of the RVS spectra. The spectroscopic pipeline will also be upgraded to derive the rotational velocities. The radial velocities of hot stars will be published when the precisions on the atmospheric parameters and on the rotational velocities, will allow to process them with the appropriate template and blend profiles.

High-velocity stars. Of the more than 7 million stars that passed successfully the above filters, 613 had absolute radial velocities larger or equal to 500 km s^{-1}. Because, this sample of high-velocity stars is very small compared to the full sample it can easily be significantly contaminated by outliers. For

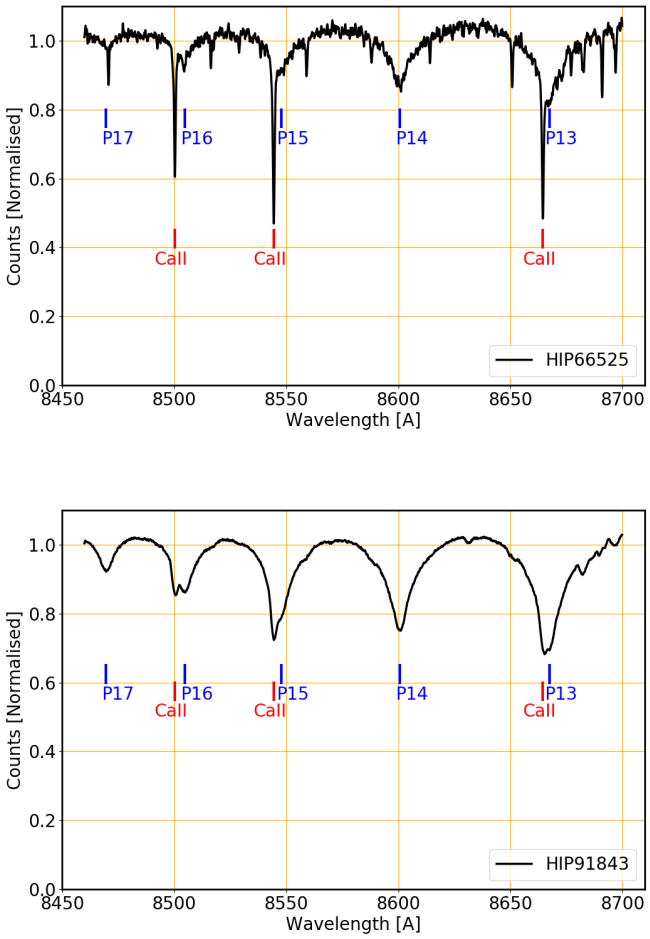

Fig. 3: RVS spectra of HIP 66525 (top) and HIP 91843 (bottom).

example, an *hypothetical* rate of 1 undetected outlier out of 10 000 stars (generating a wrong, random, uniformly distributed radial velocity) times the ~7 million total valid radial velocities, would produce about 350 false high-velocity stars, i.e. with $|V_R| \geq 500$ km s^{-1}. As a consequence, a particular attention was paid to them. Their combined spectra (see Sect. 3) were visually examined one by one and the proper locations of their Ca II lines was checked. Out of the 613 stars, 216 were considered as valid high-velocity stars and the median radial velocity of the 397 others were removed from *Gaia* DR2. Another 14 stars were rejected by astrometric and/or photometric filters, so that *Gaia* DR2 contains 202 stars with $|V_R| \geq 500$ km s^{-1}. A posteriori, it is possible to assess the contamination rate before cleaning. It was decreasing with the absolute value of the radial velocity and was of $\sim 90\%$ in the range $[950, 1000]$ km s^{-1}and $\sim 20\%$ in the range $[500, 550]$ km s^{-1}. The number of stars was rising too fast with decreasing absolute value of the velocity to extend the systematic visual inspection to slower stars. It is therefore important, when working with *Gaia* DR2 high-velocity stars, to take into account that an additional quality filter has been applied to stars faster than 500 km s^{-1}, resulting in different selection functions for the stars below and above this value.

Many stars that failed to pass one criterion, actually missed several of them. In total, 2.6 million median radial velocities were discarded for *Gaia* DR2, mostly by the above spectroscopic filters, but some also by other DPAC filters based on photometric or astrometric criteria (Gaia Collaboration et al. 2018b; Lindegren et al. 2018; Evans et al. 2018; Arenou et al. 2018).

5. The *Gaia* DR2 radial velocity catalogue

This section describes the content of the *Gaia* DR2 radial velocity catalogue, i.e. the products and their properties (Sect. 5.1) and presents the assessment of the *Gaia* DR2 radial velocity accuracy (Sect. 5.2) and precision (Sect. 5.3).

5.1. Catalogue content

Gaia DR2 contains median radial velocities for 7 224 631 stars as well as their radial velocity uncertainties, number of transits and template parameters (effective temperature, surface gravity and metallicity). The spectroscopic fields published in *Gaia* DR2 are listed in Table 1.

Table 1: Spectroscopic content of Gaia-DR2.

Field	Units	DB column name
Median radial velocity	km s^{-1}	radial_velocity
Radial velocity uncertainty	km s^{-1}	radial_velocity_error
Number of transits	transits	rv_nb_transits
Template temperature	K	rv_template_teff
Template surface gravity	dex	rv_template_logg
Template metallicity	dex	rv_template_fe_h

The spectroscopic catalogue has a full sky coverage. Figure 4 shows the distribution in Galactic coordinates of the stars with a radial velocity in *Gaia* DR2. The vast majority of the stars belong to the Milky-Way, but some bright members of the Large and Small Magellanic Cloud are also part of this release.

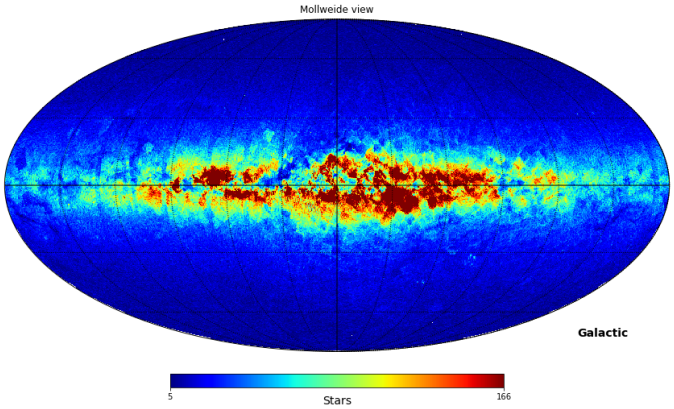

Fig. 4: Distribution on the sky of the 7 224 631 stars with a radial velocity in *Gaia* DR2. The projection is in Galactic coordinates. The Galactic Centre is in the middle of the figure and the galactic longitudes increase to the left. The pixel size is about 0.2 square degree (healpix level 7).

The external $G^{\rm ext}_{\rm RVS}$, used in *Gaia* DR2 to define the limiting magnitude of the spectroscopic pipeline, is mainly calculated from ground-based photometry (Sect. 3.3). Different catalogues

were used in different areas of the sky and with different colour-colour relations. This led to small variations of the $G_{\rm RVS}^{\rm ext}$ zero-point and therefore of the limiting magnitude of the processing, as a function of celestial coordinates. The variations are visible in the star counts as small amplitudes patterns of one to a few degree size.

Figure 5 shows the G-magnitude distribution of the stars with a radial velocity in *Gaia* DR2. For the release, the spectroscopic pipeline has processed stars down to $G_{\rm RVS}^{\rm ext}$= 12 mag. Yet, because a majority of stars are fainter in G than in $G_{\rm RVS}$ (for an un-reddened G2V star, $G-G_{\rm RVS}$= 0.65 mag), the mode of the G-magnitude distribution is located in the range $G \in [12.5, 13]$ mag. The minimum, first quartile, median, third quartile and maximum (not visible in the figure) of the distribution are respectively $G \sim 1.9, 11.7, 12.5, 13.0$ and18.3 mag.

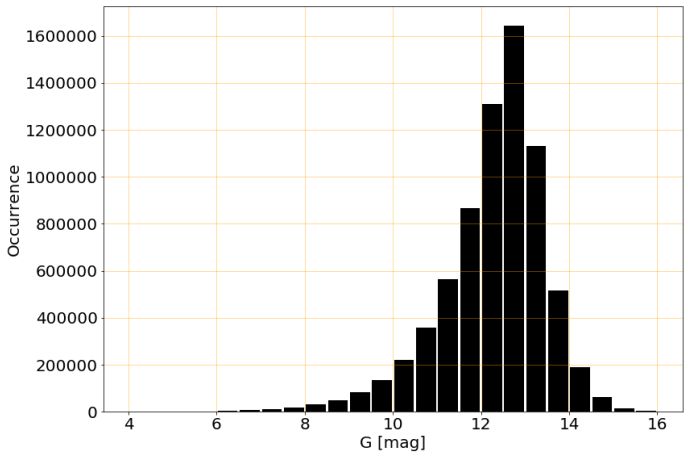

Fig. 5: G-magnitude distribution of the stars with a radial velocity published in *Gaia* DR2.

Figure 6 (top) shows the completeness of the *Gaia* DR2 radial velocities with respect to the full *Gaia* DR2 catalogue, as a function of G-magnitude. The completeness increases smoothly from $G \sim 4$ to $G \sim 11.5$ mag. The steep decrease for the faint stars is the consequence of the limiting magnitude of *Gaia* DR2 processing: $G_{\rm RVS}^{\rm ext}$= 12 mag. The sharp cut-off at $G \sim 4$ mag is due to the saturation of the core of the RVS spectra, which are then discarded by the spectroscopic pipeline. The completeness for $G \leq 12.5$ is 77.2%.

Figure 6 (bottom) shows the completeness with respect to the *Gaia* DR2 catalogue, as a function of galactic coordinates, for the stars with $G \leq 12.5$ mag. At the first order, the completeness is driven by the projected stellar density. In dense areas, the conflicts between RVS windows are more frequent, leading to a higher probability of the windows to be truncated and therefore not processed by the pipeline. As a consequence, the completeness is lower in the directions of the Galactic bulge and in the Galactic disc and rapidly increases as one moves away from the Galactic plane. A second effect, still related to stellar density, plays a role in the completeness. The number of spectra which can be simultaneously read per RVS CCDs is limited (Cropper et al. 2018). The threshold corresponds to a stellar density of about 36 000 sources per square degree. As a consequence, in dense areas, some spectra are not read on a given transit. This effect is partly mitigated by the repeated scans of the sky. A source which is not recorded on one transit, could be on the following ones. The completeness is therefore expected to increase with the successive data releases, as longer time range will be processed, e.g. 60 months for the full nominal mission versus 22 for *Gaia* DR2.

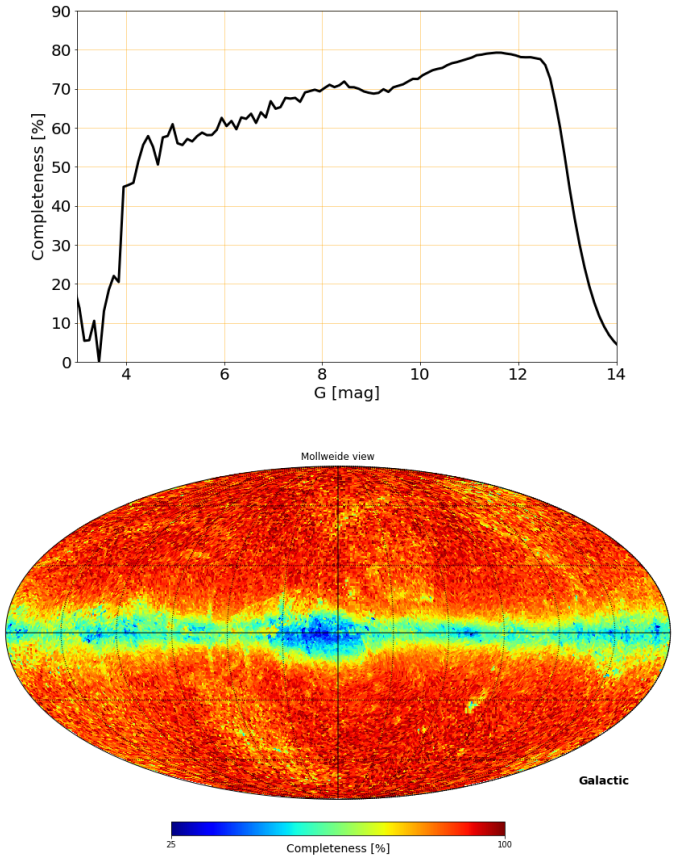

Fig. 6: Top: Completeness with respect to the full *Gaia* DR2 catalogue, as a function of G magnitude. Bottom: Completeness with respect to the *Gaia* DR2 catalogue, for the stars with $G \leq 12.5$ mag, as a function of galactic coordinates. The Galactic Centre is in the middle of the figure and the galactic longitudes increase to the left. The pixel size is ∼0.8 square degree (healpix level 6).

5.1.1. Median radial velocity

The radial velocity published in *Gaia* DR2 is the median of the radial velocities derived per transit. Some observations were not used for the calculation of the median:

- Truncated windows (caused by the overlap with the window of another star) were not processed for *Gaia* DR2 and therefore had no transit $V_{\rm R}$ derived (for that transit).
- Transits for which a spectrum was flagged as double-line spectroscopic binaries (SB2) were excluded from the calculation of the median.

A minimum of two eligible (i.e. non-truncated, non-SB2) transits was required to derive the median radial velocity of a star. The radial velocities of ∼1.6 million sources with a single eligible transit were not published in *Gaia* DR2.

Figure 7 (top) shows the map of the medians of the *Gaia* DR2 radial velocities, $\tilde{V}_{\rm R}$, as a function of galactic coordinates. The medians are calculated over healpix level 7 pixels of about

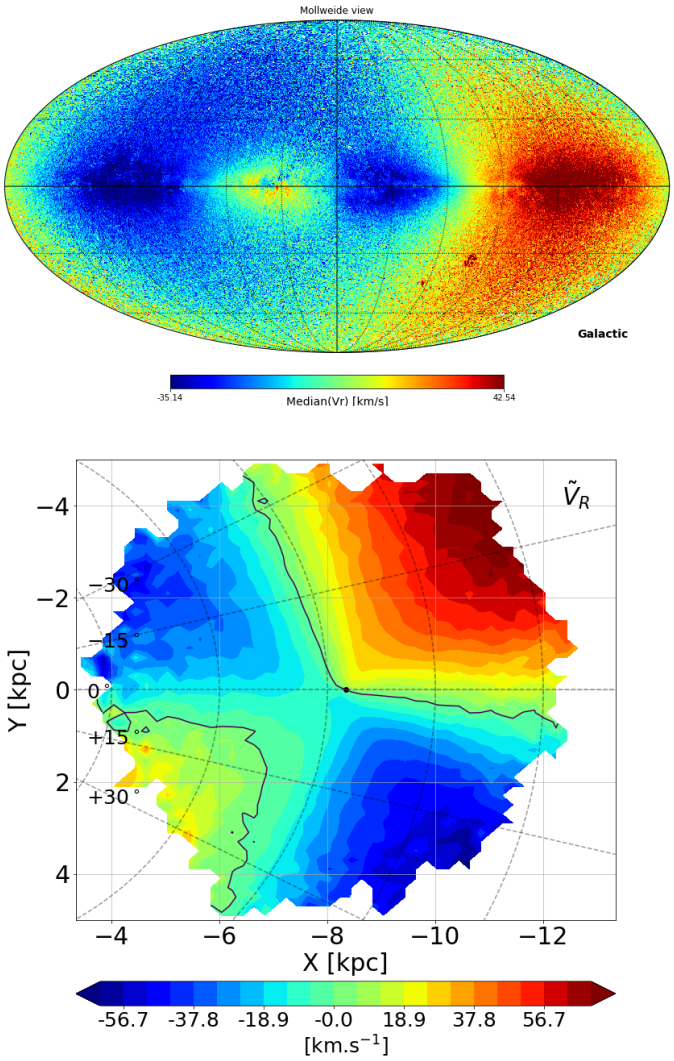

Fig. 7: Top: Map of the medians of the *Gaia* DR2 radial velocities as a function of galactic coordinates. The Galactic Centre is in the middle of the figure and the galactic longitudes increase to the left. The pixel size is ∼ 0.2 square degree (healpix level 7). Bottom: Face-on view map of the medians (over cells of 200 pc by 200 pc) of the *Gaia* DR2 radial velocities, $\tilde{V}_R$, for the Galactic disc, as seen from the north Galactic pole. The Galactic azimuths are increasing clockwise. They are labelled from −30 to +30 degrees, on the left of the map. The Sun is represented by a black dot, located at $X = -8.34$ kpc (Reid et al. 2014) and $Y = 0$ kpc. The galactic centre is located on the left side. The Milky Way is rotating clockwise. The galactic longitudes are defined counter clockwise (around the Sun). The iso-velocity contour $\tilde{V}_R = 0$ is pointed out as black lines. The map has been calculated using 5 020 596 stars, selected in a 2 kpc horizontal layer centred on the Galactic mid-plane.

0.2 square degree each (the same area as the star counts map: Fig. 4). Figure 7 (bottom) presents the face-on view map of the medians of the *Gaia* DR2 radial velocities, of the Galactic disc stars, for sources located within ±1 kpc of the Galactic mid-plane. The stars in the face-on map were also selected on the basis of their relative parallax uncertainty: $\sigma_\varpi/\varpi \leq 20\%$. The medians of the *Gaia* DR2 radial velocities are calculated over cells of 200 pc by 200 pc. Both maps show the line-of-sight-projected differential rotation of the stars of the Galaxy, as observed from the Sun. The Large and Small Magellanic Clouds also stands out clearly in the top part of Fig. 7 around $(l, b) \sim (-80°, -33°)$ and $(-57°, -44°)$ respectively.

5.1.2. Radial velocity uncertainty

The radial velocity uncertainty is calculated as the uncertainty on the median of the transit radial velocities quadratically summed with a constant term of 0.11 km s^{-1} which represents the current calibration noise floor:

$$\epsilon_{V_R} = [(\sqrt{\frac{\pi}{2N}}\sigma_{V_R^t})^2 + 0.11^2]^{0.5} \quad (1)$$

where N is the number of eligible transits used to derive the median radial velocity, $\sigma_{V_R^t} = \sqrt{\frac{1}{N-1}\sum_{i=1}^{N}(V_R^t(i) - \overline{V_R^t(i)})^2}$ the standard deviation of the eligible transit radial velocities, $V_R^t(i)$ the i^{th} transit radial velocity of the time series and $\overline{V_R^t(i)}$ the mean radial velocity.

Figure 8 shows the distribution of the radial velocity uncertainties. The first quartile, median and third quartile of the distribution are respectively: 0.55, 1.05 and 2.08 km s^{-1}.

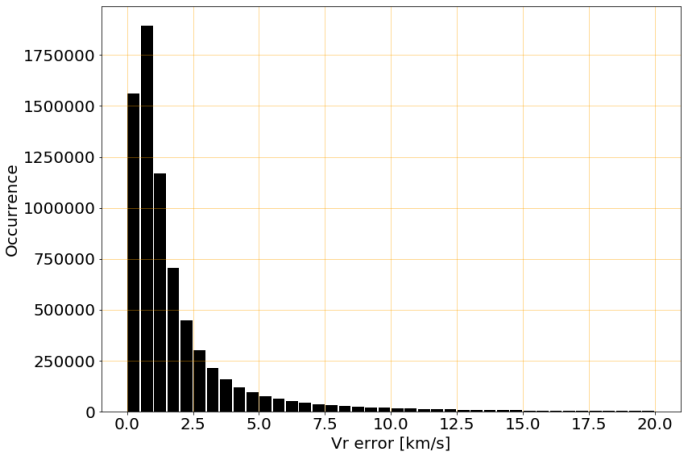

Fig. 8: Distribution of the radial velocity uncertainties.

The radial velocity uncertainty relies on the standard deviation of the time series of transit radial velocities. As described in the next section (Sect. 5.1.3), some time series are made of a few transits, in which cases the standard deviations and therefore the radial velocity uncertainties are less precise than for larger number of transits.

5.1.3. Number of transits

The number of transits published in *Gaia* DR2 , is the number of eligible transits used to compute the median radial velocity. Figure 9 (top) shows the distribution of the number of transits. It ranges from 2 (by construction) to 201, with a median number of 7.

The main driver of the number of observations for a source is the satellite scan law, which defines how many times a specific area of the sky has been monitored. During the first 28 days of the nominal mission, *Gaia* was in *"Ecliptic Pole Scanning Law"* (EPSL) and was observing each Ecliptic Pole with each telescope every 6 hours (the spin period of the satellite). The stars with large number of transits are stars close to the Ecliptic Poles which have been repeatedly monitored during the 28 days of EPSL. The second factor which defines the number of transits is the stellar density. In dense areas, the stars are closer and the probability of conflict (i.e. overlap) between RVS windows is higher. For *Gaia* DR2, overlapped windows have not

been processed and as a consequence the mean number of transits is lower in dense areas. It should be noted that the satellite scans have different orientations at different transits. Because of the very elongated geometry of the windows, it is not systematic that a star overlaps with the same neighbour at each transit. Therefore, the stellar density impacts first the number of transits before the completeness (which is also impacted, as shown in Sect. 5.1). Figure 9 (bottom) shows the distribution on the sky (galactic coordinates) of the median number of transits per ∼0.2 square degree pixel.

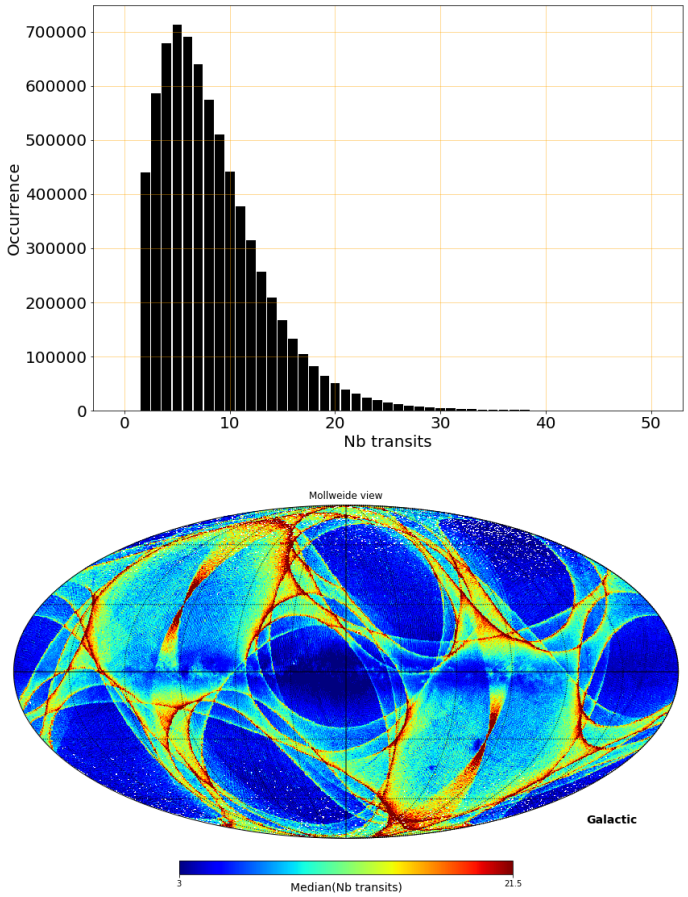

Fig. 9: Top: Distribution of the number of transits per star used to derive the median radial velocity. The full distribution extends to 201 transits. The 1053 stars (0.015% of the total) with more than 50 transits are not shown in the histogram. Bottom: Distribution of the median number of transits as a function of galactic coordinates. The Galactic Centre is in the middle of the figure and the galactic longitudes increase to the left. The pixel size is about 0.2 square degree (healpix level 7).

5.1.4. Parameters of the template

The transit radial velocities are derived by *"comparison"* (Cross-correlation or minimum distance methods, see Sartoretti et al. 2018) with a synthetic spectrum, referred to as template. The spectroscopic pipeline has two ways to select a template. If the parameters of the star are contained in the compilation of ground-based stellar parameters used by the pipeline (see Sartoretti et al. 2018), they are used to select the closest template in a library of 5256 spectra. Otherwise, the template is chosen by a dedicated module, *determineAP*, from a smaller set of 28 templates (see Sect. 3.2). Of the 7 224 631 stars, ∼ 18% had their templates selected using the ground-based compilation. Appendix A details the distributions of the parameters of the templates.

The template parameters are published in the second *Gaia* release in order to inform the users on the synthetic spectra used to derive the radial velocities. They are not meant to be used as an estimate of the stars atmospheric parameters for any other purpose. It should be noted that *Gaia* DR2 contains effective temperature estimates, derived from G, $G_{\rm BP}$ and $G_{\rm RP}$ photometry, for about 160 million stars with $T_{\rm eff} \in [3000, 10000]$ K and brighter than $G = 17$ mag (Andrae et al. 2018).

5.2. Radial velocity accuracy

The accuracy is the systematic difference between the measured values and the true values. Unfortunately, the true values of the radial velocities of the *Gaia* DR2 stars are not known. Therefore, as a proxy, five ground-based catalogues[3] are used: CU6GB (Soubiran et al. 2018), SIM (Makarov & Unwin 2015), RAVE (Kunder et al. 2017), APOGEE (Abolfathi et al. 2017) and Gaia-ESO-Survey (GES; Gilmore et al. 2012). In each case, only a subset of these catalogues has been selected, made of stars showing no radial velocity variability. Our GES validation subsample being small, it has been used only for the assessment of the accuracy as a function of the $G_{\rm RVS}$ magnitude.

The limitation of the comparison to external catalogues, is that they can, of course, also be affected by their own biases. Therefore, when a systematic difference is observed between *Gaia* DR2 and a catalogue, it could come from the former, the latter or both. Using several external catalogues is meant to help (pending that they do not share some systematic(s)). It should be noted that, even if the true accuracy is difficult to assess from the comparison of different catalogues, it is of interest to know their relative differences, for e.g. combining data from these catalogues or comparing results obtained independently with them.

CU6GB (Soubiran et al. 2018) is a ground-based radial velocity catalogue produced by the *Gaia* DPAC. The zero-point of the radial velocities of the CU6GB catalogue (i.e. its accuracy) has been assessed by comparing measured radial velocities of asteroids to celestial mechanics predictions. The zero-point of CU6GB is 38 ± 5 m s^{-1}.

As *estimator of the accuracy*, we use the median of the radial velocity residuals, $V_{\rm R}^{\rm res}$ (i.e. Gaia DR2 minus ground based catalogue). The lower and upper 1-σ uncertainties on the estimate of the accuracy are calculated respectively as:

$$\epsilon_{\rm acc}^{\rm low} = \sqrt{\frac{\pi}{2N_{V_{\rm R}^{\rm res}}}}(\tilde{V}_{\rm R}^{\rm res} - Per(V_{\rm R}^{\rm res}, 15.85)) \quad (2)$$

$$\epsilon_{\rm acc}^{\rm upp} = \sqrt{\frac{\pi}{2N_{V_{\rm R}^{\rm res}}}}(Per(V_{\rm R}^{\rm res}, 84.15) - \tilde{V}_{\rm R}^{\rm res}) \quad (3)$$

where $N_{V_{\rm R}^{\rm res}}$ is the number of radial velocity residuals, $\tilde{V}_{\rm R}^{\rm res}$ the median of the radial velocity residuals and $Per(V_{\rm R}^{\rm res}, 15.85)$ and $Per(V_{\rm R}^{\rm res}, 84.15)$ respectively the 15.85$^{\rm th}$ and 84.15$^{\rm th}$ percentiles of the distribution of radial velocity residuals. In the following sections, the accuracy is studied as a function of different parameters (e.g. $G_{\rm RVS}^{\rm ext}$, $G_{\rm RVS}^{\rm int}$, $T_{\rm eff}$, $\log g$). The comparison samples are

[3] Arenou et al. (2018) also compared the *Gaia* DR2 radial velocities to the first GALAH data release (Kos et al. 2017; Martell et al. 2017). The second GALAH data release (Buder et al. 2018; Zwitter et al. 2018) was published after the completion of the validation of *Gaia* DR2.

therefore divided by bins of the considered quantities. In these cases, a minimum of 20 stars per bin is required to calculate the median of the radial velocity residuals.

Table 2 presents the median radial velocity residuals derived for the five ground-based catalogues. Gaia-DR2 shows a small 2.4-σ level offset of -12 m s^{-1} with respect to CU6GB. The CU6GB stars brighter than or equal to $G_{\rm RVS}^{\rm ext}$= 9 mag, and showing no variability, were used in the wavelength calibration procedure to set the wavelength zero-point of each configuration: i.e. field-of-view/CCD/trending epoch (Sartoretti et al. 2018). It is a good sanity check for the pipeline, that neither the wavelength calibration, nor the subsequent modules did modify significantly the global radial velocity zero-point defined by the CU6GB catalogue. Gaia-DR2 shows a positive global offset of about +200 to +300 m s^{-1} with respect to the SIM, RAVE, APOGEE and GES stars. Yet, as discussed in the following sections, the origin of these offsets varies partially from one catalogue to another.

Table 2: Median radial velocity residuals derived from the comparison of *Gaia* DR2 with ground-based catalogues. $N_{\rm stars}$ (Col. 3) is the number of stars selected to calculate the median residuals.

Catalogue	Median $V_{\rm R}^{\rm res}$ [km s^{-1}]	$N_{\rm stars}$
CU6GB	-0.012 -0.005/+0.005	4083
SIM	+0.264 -0.015/+0.014	640
RAVE	+0.295 -0.013/+0.013	9127
APOGEE	+0.233 -0.011/+0.013	8124
GES	+0.236 -0.043/+0.049	2120

5.2.1. Accuracy versus number of transits

Figure 10 shows the median radial velocity residuals as a function of the number of eligible transits. In general, the accuracy is not expected to improve or vary with the number of measures. Yet, in *Gaia* DR2, the number of transits is very correlated with the location of the stars on the sky (bottom part of Fig. 9). Therefore, potential spatial biases could have been propagated to the number of transits. *Gaia* DR2 shows no significant trend or discontinuity with respect to the CU6GB (which covers the full celestial sphere), SIM or APOGEE datasets. The median of the residuals with respect to the RAVE dataset shows a 1-2σ upward jump over the range 22 to 24 transits. This feature is not present in the other datasets and remains compatible with statistical fluctuations. The accuracy as a function of the position on the sky is directly assessed in Sect. 5.2.7.

5.2.2. Accurcay versus $G_{\rm RVS}$

Figure 11 (top) shows the median radial velocity residuals as a function of the *external* $G_{\rm RVS}^{\rm ext}$ magnitude. Over the magnitude range [7, 9] mag, *Gaia* DR2 shows no significant offset nor trend with respect to the CU6GB or APOGEE stars and it shows a nearly constant offset (similar to the global offset reported in Sect. 5.2) with respect to SIM and RAVE stars. For fainter stars, beyond $G_{\rm RVS}^{\rm ext}$~9-10 mag, the *Gaia* DR2 velocities exhibit an increasing positive offset with respect to all the catalogues, reaching about ~500 m s^{-1} at $G_{\rm RVS}^{\rm ext}$~11.75. The trend is also visible in the median of the residuals as a function of the *internal* $G_{\rm RVS}^{\rm int}$ magnitude, which is derived from the flux recorded in the RVS windows (middle part of Fig. 11).

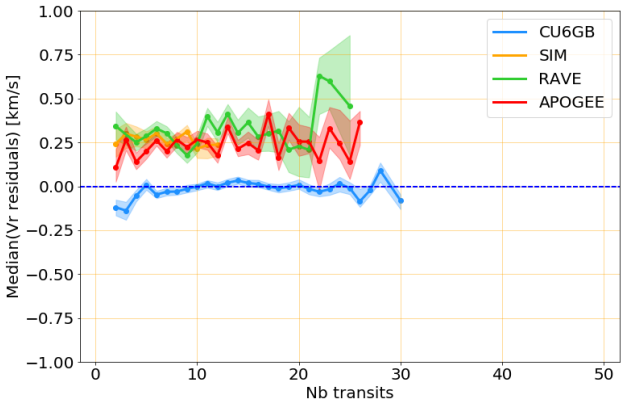

Fig. 10: Median radial velocity residuals as a function of the number of transits. The lower and upper 1-σ uncertainties on the measures of the medians are represented as shaded areas.

Each validation catalogue contains a mix of stars of different temperatures, gravities and metallicities, whose proportion could change with magnitude. In order to check that the observed trend at faint magnitude was not caused by e.g. a differential effect between dwarfs and giants whose proportion could be function of magnitude, a sub-sample of 3220 solar metallicity giant stars was selected, fulfilling the criteria: $T_{\rm eff}$ in [4500, 5000] K, $\log g$ in [2.3, 3.0] and [Fe/H] in [-0.3, 0.3] dex. Figure 11 (bottom) presents the median radial velocity residuals as a function of the external $G_{\rm RVS}^{\rm ext}$ for the giant star sub-sample. As for the full validation sample, at magnitude brighter than $G_{\rm RVS}^{\rm ext}$ ~ 9 (APOGEE) or 10 mag (RAVE) the offset is constant. At fainter magnitude the median residuals exhibit a positive gradient with magnitude.

The same trend is observed with all the validation catalogues, for both the external and internal $G_{\rm RVS}$ magnitudes and for the full sample as well as for a subset of similar giant stars. The probability is therefore high, that the effect is in the *Gaia* DR2 data. The origin of the trend is under investigation. The first lead explored was the Charge Transfer Inefficiency (CTI), but this hypothesis has been dismissed (see Appendix B). The calibrations of the wavelengths and of the instrumental profile are now scrutinised to assess if they could play a role in the trend. The aim is to understand, model and correct for the trend in *Gaia* DR3.

It should be noted that while SIM and RAVE validation samples present already an offset for bright stars (which increases further for RAVE faint stars), APOGEE bright stars present little offset. The global offset between *Gaia* DR2 and APOGEE reported in Sect. 5.2 is mainly due to the prevalence of faint stars in this validation sample, while there is a global offset with respect to RAVE and SIM stars. Table 3 presents the median radial velocity residuals for the subsets of stars, from the validation catalogues, brighter than $G_{\rm RVS}^{\rm ext}$ = 9 mag.

5.2.3. Accuracy versus temperature

Figure 12 (top) presents the median radial velocity residuals as a function of the star effective temperature[4] (left) and as a function of the template effective temperature (right). Both the CU6GB

[4] The effective temperatures, surface gravities and metallicities used here and in the following sections come from the compilation of ground-based catalogues used by the spectroscopic pipeline (Sartoretti et al. 2018). Stellar parameters from different catalogues have been usually

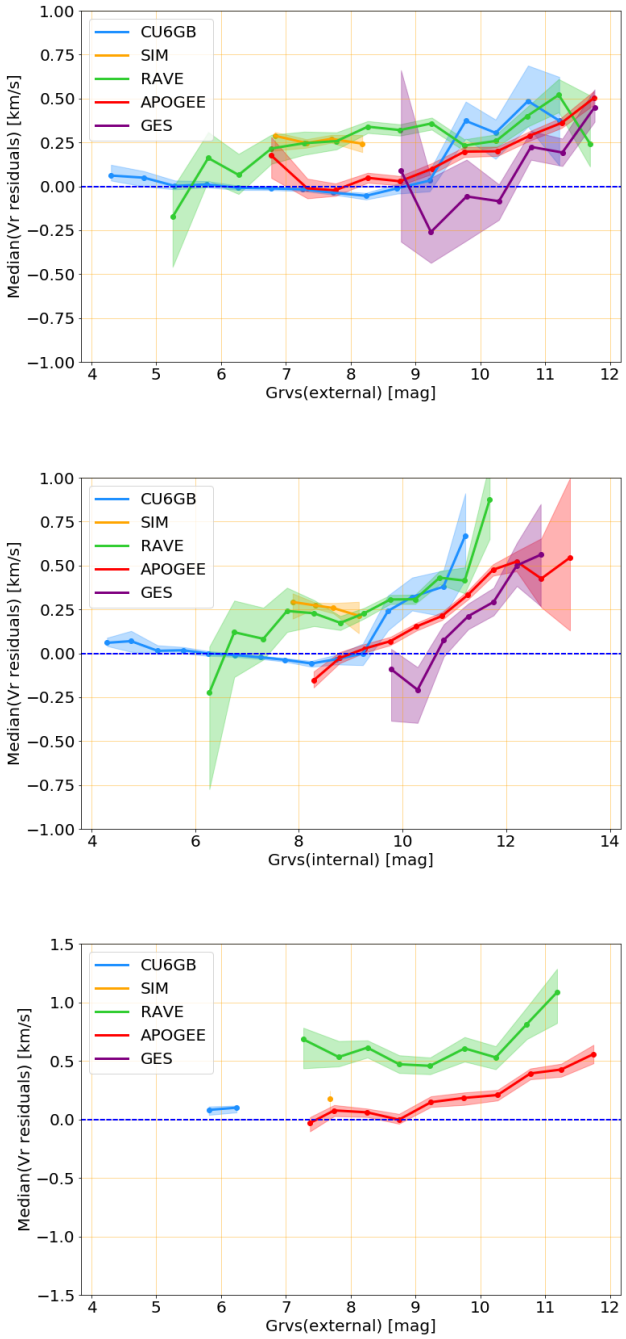

Fig. 11: Top: Median radial velocity residuals as a function of the external G^{ext}_{RVS} magnitude. Middle: Median radial velocity residuals as a function of the internal G^{int}_{RVS} magnitude. Bottom: Median radial velocity residuals as a function of the internal G^{int}_{RVS} magnitude, for a subset of giant stars. The lower and upper 1-σ uncertainties on the measures of the medians are represented as shaded areas.

and the RAVE validation samples show a drop of the median residuals by about 500 m s^{-1} for cool stars, from 4750-4500 to 4000 K. Over the same temperature range, the APOGEE sample exhibits flat residuals. Beyond, ~5500 K the median residuals of the APOGEE sample show a smooth decrease of about 200 m s^{-1}.

Around 4500 K (where the CU6GB and RAVE curves show an inflection), the RVS spectra are dominated by the Ca II triplet. The morphology of the spectra evolves smoothly with the effective temperature. There is no sudden change in the RVS spectra which would produce the inflection observed in the two curves (but not in the APOGEE one).

Similar radial velocity offsets between M-K and hotter spectral types have been reported in the literature, when comparing measures from different spectrographs. In particular Soubiran et al. (2018) observe jumps of ~ -100 m.s^{-1} and $\sim +300$ m.s^{-1} around $J-K \sim 0.75$ mag, respectively for Sophie (Perruchot et al. 2008) minus Harps (Queloz et al. 2001; Mayor et al. 2003) and Sophie minus Elodie (Baranne et al. 1996) radial velocities. The authors suspect that the jumps are caused by the use, in the pipelines of the 3 instruments, of different masks with different radial velocity zero-points.

Table 3: Median radial velocity residuals derived from the comparison of *Gaia* DR2 with stars from the ground-based catalogues brighter than $G^{ext}_{RVS} = 9$ mag. N_{stars} (Col. 3) is the number of stars selected to calculate the median residuals.

Catalogue	Median V^{res}_R [km s^{-1}]	N_{stars}
CU6GB	−0.017 −0.005/+0.005	3805
SIM	+0.264 −0.015/+0.014	640
RAVE	+0.282 −0.019/+0.019	3838
APOGEE	+0.024 −0.015/+0.017	1141
GES	−0.184 −0.418/+0.254	63

5.2.4. Accuracy versus gravity

Figure 12 (middle) presents the median radial velocity residuals as a function of the star surface gravity (left) and as a function of the template surface gravity (right). The main feature is a smooth decrease of the median residuals of the *Gaia* DR2 data versus RAVE by about 700 m s^{-1} between $\log g \sim 2.5$ and $\log g \sim 1$. The effect is not seen in the other validation samples, in particular APOGEE which also extends to low gravities.

5.2.5. Accuracy versus metallicity

Figure 12 (bottom) presents the median radial velocity residuals as a function of the star metallicity (left) and as a function of the template metallicity (right). The median residuals of the *Gaia* DR2 versus RAVE velocities show a positive trend with metallicity which reaches ~750 m s^{-1} for the most metal-rich sources. On the metal-poor side, the CU6GB sample shows a negative offset of about −500 m s^{-1} for the stars whose velocity has been calculated with templates having a metallicity of −1.5 dex. The APOGEE validation sample shows no significant trend with metallicity.

5.2.6. Accuracy versus velocity

Figure 13 presents the median radial velocity residuals as a function of the star velocity. The residuals of the *Gaia* DR2 versus RAVE velocities decrease by about 600-700 m s^{-1} from +25 km s^{-1} to −125 km s^{-1} and show a symmetric behaviour at positive velocities. The small number of high velocity stars

derived with different methods and therefore show some heterogeneity in their zero-points and scales.

Fig. 12: Top: Median radial velocity residuals as a function of the effective temperature of the stars (left) and of the templates (right). Middle: Median radial velocity residuals as a function of the surface gravity of the stars (left) and of the templates (right). Bottom: Median radial velocity residuals as a function of the metallicity of the stars (left) and of the templates (right). The lower and upper 1-σ uncertainties on the measures of the medians are represented as shaded areas.

in our validation datasets prevents from deriving precise median residuals outside $[-175, +175]$ km s^{-1}, whereas the pipeline derives radial velocities in the range $[-1000, +1000]$ km s^{-1}. The individual radial velocity residuals (Figure 14) provide a view on a broader velocity interval. The individual residuals do not show any strong offset or trend over the interval $[-400, 400]$ km s^{-1}. The fastest validation star has a radial velocity of 552.6 km s^{-1} in our RAVE list and 553.5 km s^{-1} in *Gaia* DR2. As described in Sect. 4, the combined spectra of the stars with radial velocities $|V_R| \geq 500$ km s^{-1} were visually inspected one by one and those considered as *false high-velocity stars* were discarded from *Gaia* DR2.

5.2.7. Accuracy versus sky coordinates

Figure 15 presents the sky map, in galactic coordinates, of the median radial velocity residuals per pixel of ~54 square degrees (healpix level 3). To increase the number of validation stars, the 5 ground-based catalogues presented in Sect. 5.2 have been complemented with 5820 stars from the Extended Hipparcos Compilation (XHIP; Anderson & Francis 2012). Nonetheless, for a

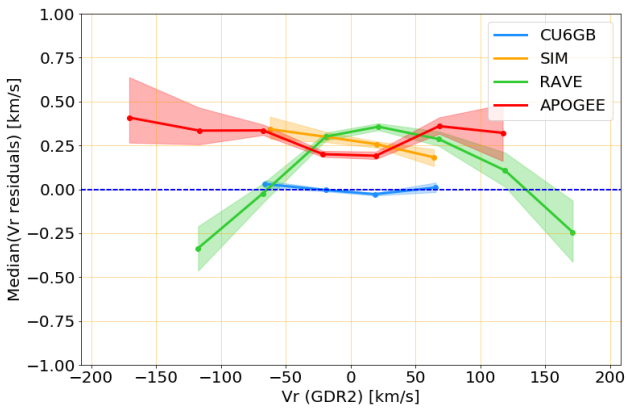

Fig. 13: Median radial velocity residuals as a function of the *Gaia* DR2 radial velocity. The lower and upper 1-σ uncertainties on the measures of the medians are represented as shaded areas.

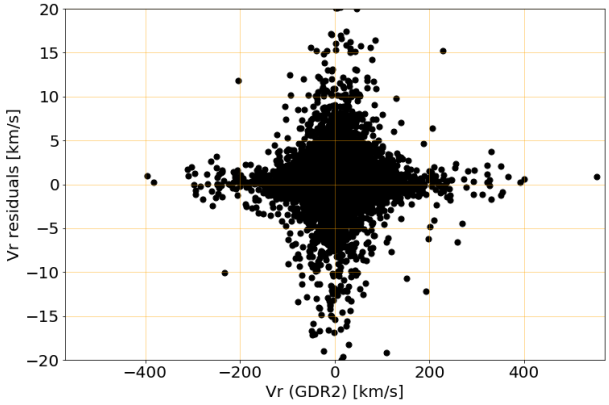

Fig. 14: Individual radial velocity residuals as a function of the *Gaia* DR2 radial velocity, for 24 063 validation stars. Thirty one validation stars, with an absolute value of the radial velocity residual larger than 20 km s^{-1}, are not displayed. The dots extend to larger residuals at small absolute velocities than at larger ones. This is a visual effect due to the fact that small absolute velocities are much more densely populated than larger ones and therefore the wings of the distribution of residuals are probed to much larger values.

few pixels, the minimum number stars required to calculate the median, lowered here to 5 stars per pixel, was not reached. Those pixels appear in white on the map. To produce the map, the validation datasets have been corrected for their respective median radial velocity residuals (see Table 2) and then combined. This explains why the distribution of median radial velocity residuals is roughly centred on zero. The 2$^{\rm nd}$ and 98$^{\rm th}$ percentiles of the distribution are respectively −0.34 and +0.29 km s^{-1}, while the extrema are −0.81 and +0.64 km s^{-1}.

Xhip radial velocities come from the compilation of 47 different sources (Anderson & Francis 2012) with different radial velocity zero-points. This makes the median of the residuals of *Gaia* DR2 versus Xhip more difficult to interpret and this is why it was not used in the previous sections to assess the accuracy of *Gaia* DR2. The estimation of the *Gaia* radial velocity accuracy as a function of sky coordinates involves much more cells (i.e. 768) than the previous diagnostics. Xhip was therefore combined

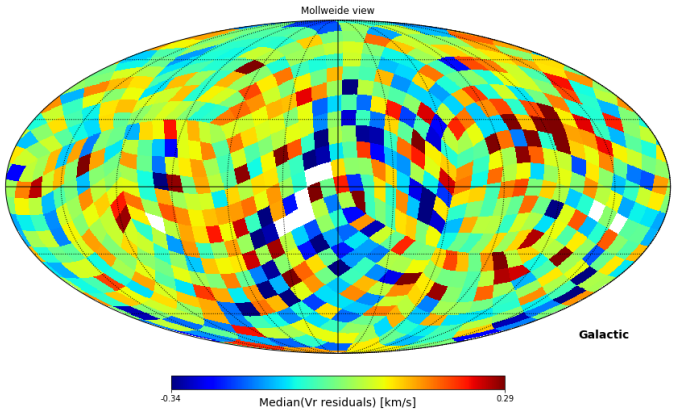

Fig. 15: Sky map, in galactic coordinates, of the median radial velocity residuals per pixel of ∼54 square degrees (healpix level 3). The Galactic Centre is in the middle of the figure and the galactic longitudes increase to the left.

to the 5 other ground-based catalogues to increase the global statistics, but also because it provides a full sky coverage. To test how variations in the Xhip velocity zero-points could affect the assessment of *Gaia* DR2 spatial systematics, the same diagnostics was run without the Xhip dataset. This resulted in a very similar sky pattern and statistics (minimum, 2$^{\rm nd}$ and 98$^{\rm th}$ percentiles and maximum of the distribution, respectively: −0.86, −0.38, +0.35 and +1.23 km s^{-1}), but ∼10% of the sky with less than 5 stars per pixel and therefore without a calculated median.

5.2.8. Accuracy: summary

The main systematic found in the *Gaia* DR2 radial velocities is a trend with magnitude, which starts around $G_{\rm RVS}$ ∼9-10 mag and reaches about +500 m s^{-1} at $G^{\rm ext}_{\rm RVS}$ = 11.75 mag (see Sect. 5.2.2). In addition to this trend, *Gaia* DR2 shows offsets of about +250/+300 m s^{-1} with respect to the SIM and RAVE validation samples. Other offsets, specific to a range of parameter and to a catalogue have been identified (see previous sections for the details). They do not exceed a few 100s m s^{-1}.

5.3. Radial velocity precision

Two different datasets and statistical estimators are used to assess the precision of the *Gaia* DR2 radial velocities.

The first dataset is made of a compilation of 3 ground-based catalogues, CU6GB, SIM and APOGEE (this last restricted to the stars with $G^{\rm ext}_{\rm RVS}$> 8.5 mag), which have better internal precisions than *Gaia* DR2 (see Sect. 5.3.2). Since the different catalogues have small relative offsets, they were first corrected for their median radial velocity residuals (−0.012, +0.264 and +0.268 km s^{-1} respectively for the CU6GB, SIM and APOGEE datasets) before being combined in a single dataset, hereafter referred to as the GB[5] validation dataset. It consists of 12 119 stars.

With this dataset, the *Gaia* DR2 radial velocity precision is calculated as the robust dispersion of the radial velocity residuals:

$$\sigma^{\rm GB}_{V_{\rm R}} = \frac{Per(V^{\rm res}_{\rm R}, 84.15) - Per(V^{\rm res}_{\rm R}, 15.85)}{2} \quad (4)$$

[5] standing for ground-based.

where $Per(V_{\rm R}^{\rm res}, 15.85)$ and $Per(V_{\rm R}^{\rm res}, 84.15)$ are respectively the 15.85$^{\rm th}$ and 84.15$^{\rm th}$ percentiles of the distribution of radial velocity residuals: $V_{\rm R}^{\rm res} = V_{\rm R}^{\rm GDR2} - V_{\rm R}^{\rm GB}$. The lower and upper 1-$\sigma$ uncertainties on the precision are calculated as:

$$\epsilon^{\rm low}_{\sigma^{\rm GB}_{V_{\rm R}}} = \frac{\sqrt{2\pi}}{e^{-0.5}} \sqrt{\frac{0.1585 \times 0.683}{N_{V_{\rm R}^{\rm res}}}} (\tilde{V}_{\rm R}^{\rm res} - Per(V_{\rm R}^{\rm res}, 15.85)) \quad (5)$$

$$\epsilon^{\rm upp}_{\sigma^{\rm GB}_{V_{\rm R}}} = \frac{\sqrt{2\pi}}{e^{-0.5}} \sqrt{\frac{0.1585 \times 0.683}{N_{V_{\rm R}^{\rm res}}}} (Per(V_{\rm R}^{\rm res}, 84.15) - \tilde{V}_{\rm R}^{\rm res}) \quad (6)$$

where $\tilde{V}_{\rm R}^{\rm res}$ is the median of the radial velocity residuals and $N_{V_{\rm R}^{\rm res}}$ the number of radial velocity residuals.

The second dataset is made of all the stars with a radial velocity published in *Gaia* DR2 and is hereafter referred to as the full dataset. With this dataset, the estimator of the precision is the median of the radial velocity uncertainties (Sect. 5.1.2):

$$\sigma^{\rm Full}_{V_{\rm R}} = \tilde{\epsilon}_{V_{\rm R}} \quad (7)$$

and the lower and upper 1-σ uncertainties on the precision are calculated as:

$$\epsilon^{\rm low}_{\sigma^{\rm Full}_{V_{\rm R}}} = \sqrt{\frac{\pi}{2N_{\epsilon_{V_{\rm R}}}}} (\tilde{\epsilon}_{V_{\rm R}} - Per(\epsilon_{V_{\rm R}}, 15.85)) \quad (8)$$

$$\epsilon^{\rm upp}_{\sigma^{\rm Full}_{V_{\rm R}}} = \sqrt{\frac{\pi}{2N_{\epsilon_{V_{\rm R}}}}} (Per(\epsilon_{V_{\rm R}}, 84.15) - \tilde{\epsilon}_{V_{\rm R}}) \quad (9)$$

where $N_{\epsilon_{V_{\rm R}}}$ is the number of individual radial velocity uncertainties and $\tilde{\epsilon}_{V_{\rm R}}$, $Per(\epsilon_{V_{\rm R}}, 15.85)$ and $Per(\epsilon_{V_{\rm R}}, 84.15)$ respectively the median, 15.85$^{\rm th}$ and 84.15$^{\rm th}$ percentiles of the distribution of radial velocity uncertainties. The radial velocity uncertainty, $\epsilon_{V_{\rm R}}$, is function of the standard deviation of the time series of transit radial velocities (see equation (1)). The precision derived from the full validation dataset is therefore proportional to the scatter of the transit radial velocities.

Although the full dataset is made of the 7.2 million stars, the effective temperature, surface gravity and metallicity are known respectively for only 1.3, 0.4 and 0.4 million stars (from a compilation of ground-based catalogues). The assessment of the radial velocity precision as a function of these parameters is therefore limited to these sub-samples.

The two validation datasets and the two estimators of the precision are complementary, in the sense where they are sensitive to different aspects. The stars in the GB dataset have been selected on the basis of multiple ground-based observations to be as clean as possible of radial velocity variables. The full dataset contains all the 7 224 631 stars of the *Gaia* DR2 spectroscopic catalogue, which includes a proportion of undetected multiple and variable stars, even if the filters applied on the suspected SB2 and on the radial velocity uncertainty (Sect. 4) should have removed the bulk of the large amplitude velocity variables. The GB precision will account for some potential differential effects, like e.g. possible systematic offset between giant and dwarf stars. The full dataset precision, which relies on the scatter of the transit radial velocities of each source, is not sensitive to the possible systematics between different groups of sources.

The GB dataset is only made of 12 119 stars. It is used, together with the full dataset, to assess the precision as a function of magnitude (Sect. 5.3.2). The GB dataset is too small to assess the precision as a function of two parameters simultaneously. Therefore, when assessing the precision as a function of magnitude and number of transits (Sect. 5.3.3), magnitude and effective temperature (Sect. 5.3.4), magnitude and surface gravity (Sect. 5.3.5) or magnitude and metallicity (Sect. 5.3.6), only the full sample is used.

5.3.1. Comparing the precision estimators

To compare the estimates of the precision derived with the robust dispersion of the residuals (Eq. 4) on the one hand and with the median of the radial velocity uncertainties (Eq. 7) on the other hand, both estimators were applied to the same subset of CU6GB stars. Figure 16 shows the *external* (relying on the residuals) and *internal* (relying on the uncertainties) precisions as a function of $G_{\rm RVS}^{\rm ext}$ magnitude. Within the uncertainties, the two estimators of the precision are in good agreement.

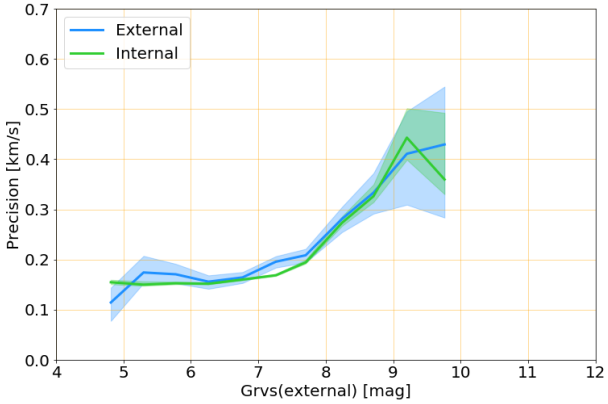

Fig. 16: Comparison of the external and internal precisions, respectively estimated using Eq. 4 and Eq. 7, as a function of $G_{\rm RVS}^{\rm ext}$ magnitude, for the CU6GB validation stars.

5.3.2. Precision versus magnitude

Figure 17 (top) shows the robust dispersion of the radial velocity residuals (Eq. 4), as a function of the external $G_{\rm RVS}^{\rm ext}$ magnitude, for *Gaia* DR2 versus the CU6GB, SIM, RAVE, APOGEE and GB validation datasets. The typical uncertainties of the CU6GB and SIM datasets are of the order of a few 10s m s^{-1} (Soubiran et al. 2018; Makarov & Unwin 2015). This is significantly smaller than the radial velocity residuals derived when comparing *Gaia* DR2 to these two datasets. Their uncertainties only contribute to a few percents of the measured residuals, which could therefore be used as an estimate of *Gaia* DR2 precision. For $G_{\rm RVS}^{\rm ext} \in \sim [8.5, 11]$ mag, the residuals of *Gaia* DR2 versus CU6GB are very similar to those versus APOGEE. This indicates that APOGEE uncertainties have a very small contribution to the derived residuals. For $G_{\rm RVS}^{\rm ext} \lesssim 8.5$ mag, the *Gaia* DR2-APOGEE residuals reach a plateau, indicative of a more significant contribution of APOGEE uncertainties to the residuals. As a consequence, only APOGEE stars fainter than $G_{\rm RVS}^{\rm ext} = 8.5$ mag were included in the GB dataset (see Sect. 5.3).The residuals with respect to the RAVE dataset include a significant contribution of RAVE uncertainties, which is why the RAVE stars were not included in the GB dataset.

Figure 17 (bottom) compares the *Gaia* DR2 radial velocity precisions as a function of the external $G_{\rm RVS}^{\rm ext}$ magnitude, estimated with the GB dataset and the full dataset. The precision

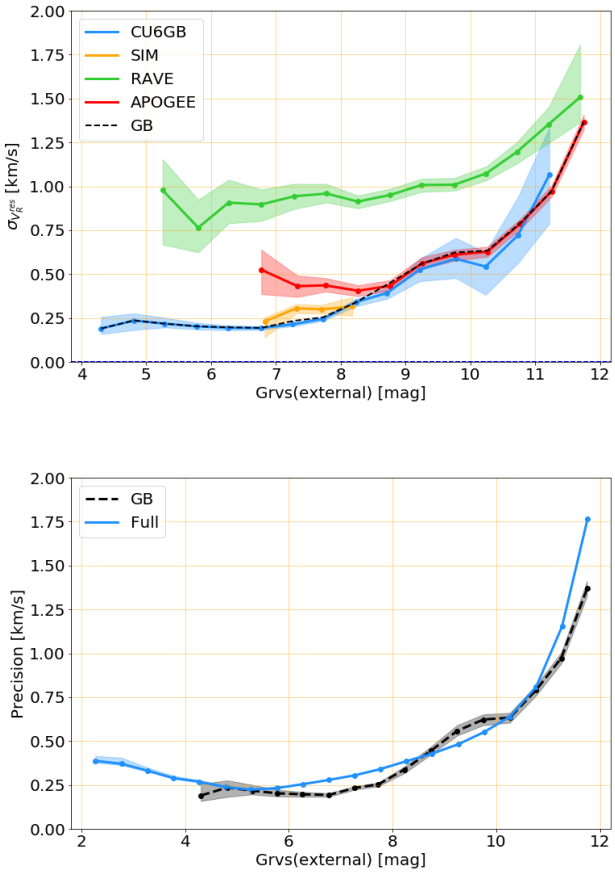

Fig. 17: Top: Robust dispersion of the radial velocity residuals as a function of the external $G_{\rm RVS}^{\rm ext}$ magnitude, for *Gaia* DR2 versus the CU6GB, SIM, RAVE, APOGEE and GB validation datasets. Bottom: Comparison of the precisions as a function of $G_{\rm RVS}^{\rm ext}$ magnitude, estimated with the GB dataset (dashed black line) and the full dataset (blue line). The lower and upper 1-σ uncertainties on the measures of the robust dispersion are represented as shaded areas.

derived using the CU6GB sample reaches ~200-250 m s^{-1} for the stars with $G_{\rm RVS}^{\rm ext} \in [4, 8]$ mag, close to the precision obtained with the full dataset: $\sim 220 - 350$ m s^{-1}. This is about 3 to 5 times more precise than the pre-launch specification, which was 1 km s^{-1}. In this range of magnitude, the *Gaia* DR2 radial velocity precision is limited by the precision of the calibrations and in particular of the wavelength calibration. From $G_{\rm RVS}^{\rm ext} \sim 5$ mag, some spectra begin to be partially saturated. The saturation increases with decreasing magnitude and as a consequence the radial velocity precision deteriorates. At $G_{\rm RVS}^{\rm ext} = 11.75$ mag, the GB dataset yield a *Gaia* DR2 precision of ~1.4 km s^{-1}. The precision derived with the full sample is slightly worse, i.e. 1.8 km s^{-1}, probably because of the larger proportion of unfiltered radial velocity variables.

5.3.3. Precision versus magnitude and number of transits

Figure 18 presents the radial velocity precision as a function of $G_{\rm RVS}^{\rm ext}$ magnitude and number of transits (the different curves), estimated with the full validation dataset. As expected, the precision improves with the number of transits. For example, at $G_{\rm RVS}^{\rm ext} = 11.75$ mag, the precision improves from ~ 2.2 to ~ 0.9 km s^{-1}, between 4 (dark blue line) and 37 transits (purple line).

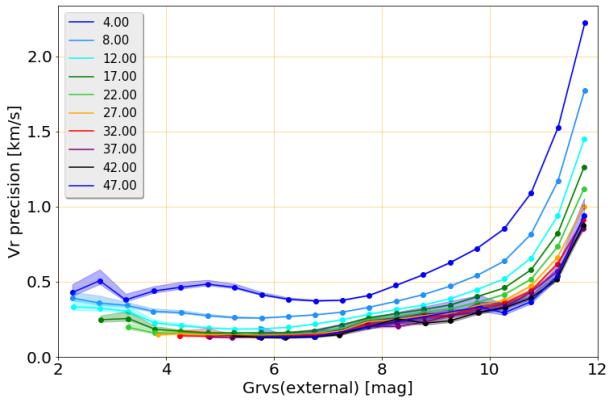

Fig. 18: Radial velocity precision as a function of $G_{\rm RVS}^{\rm ext}$ magnitude and number of transits. Each curve corresponds to an interval of 5 transits: e.g. [2, 6] transits (dark blue), [7, 11] transits (blue). The mean number of transits of each interval is given in the legend. The lower and upper 1-σ uncertainties on the measures of the precision are represented as shaded areas.

5.3.4. Precision versus magnitude and effective temperature

Figure 19 (top left) presents the *Gaia* DR2 precision as a function of the external $G_{\rm RVS}^{\rm ext}$ magnitude and effective temperature (the different curves), assessed using the 1.3 million stars from the full dataset with known $T_{\rm eff}$. The radial velocity precision improves as the effective temperature decreases. This is the direct consequence of the evolution of the morphology of the spectra with temperature. As it decreases, the weak neutral lines become on average stronger, carrying more information to derive the radial velocity. This is illustrated by Fig. 20 which compares the spectra of HIP46933 ($T_{\rm eff} = 4487$ K, $\log g = 4.22$, [Fe/H] $= -0.24$ dex; Adibekyan et al. 2012) and HIP84551 ($T_{\rm eff} = 6517$ K, $\log g = 4.20$, [Fe/H] $= +0.18$ dex; Adibekyan et al. 2012). At $G_{\rm RVS}^{\rm ext} = 11.75$ mag, the precision is ~ 2.5 km s^{-1} at $T_{\rm eff} \sim 6650$ K, ~ 1.5 km s^{-1} at $T_{\rm eff} \sim 5800$ K and ~ 1.1 km s^{-1} at $T_{\rm eff} \sim 3900$ K.

The top right frame in Figure 19 is similar to the top left frame, with the curves corresponding to different interval of effective temperatures of the templates used to process the stars (rather than interval of effective temperature of the stars). Globally, the precision improves as the effective temperature of the template decreases. Locally, some adjacent curves could show the opposite behaviour. For example, a better precision is obtained for the stars processed with a $T_{\rm eff}^{\rm tpl} = 6750$ K template (red curve), than with a $T_{\rm eff}^{\rm tpl} = 6500$ K template (orange curve). The sub-library used by the software module *determineAP* includes a synthetic spectrum with $T_{\rm eff}^{\rm tpl} = 6500$ K, but none with $T_{\rm eff}^{\rm tpl} = 6750$ K. Therefore, stars which have been processed with a $T_{\rm eff}^{\rm tpl} = 6750$ K template all had atmospheric parameters included in the compilation of ground-based catalogues. Those processed with a $T_{\rm eff}^{\rm tpl} = 6500$ K template are in majority not included in the ground-based compilation and their templates have been selected by *determineAP*. The stars whose templates have been selected by *determineAP* suffer from a larger template mismatch

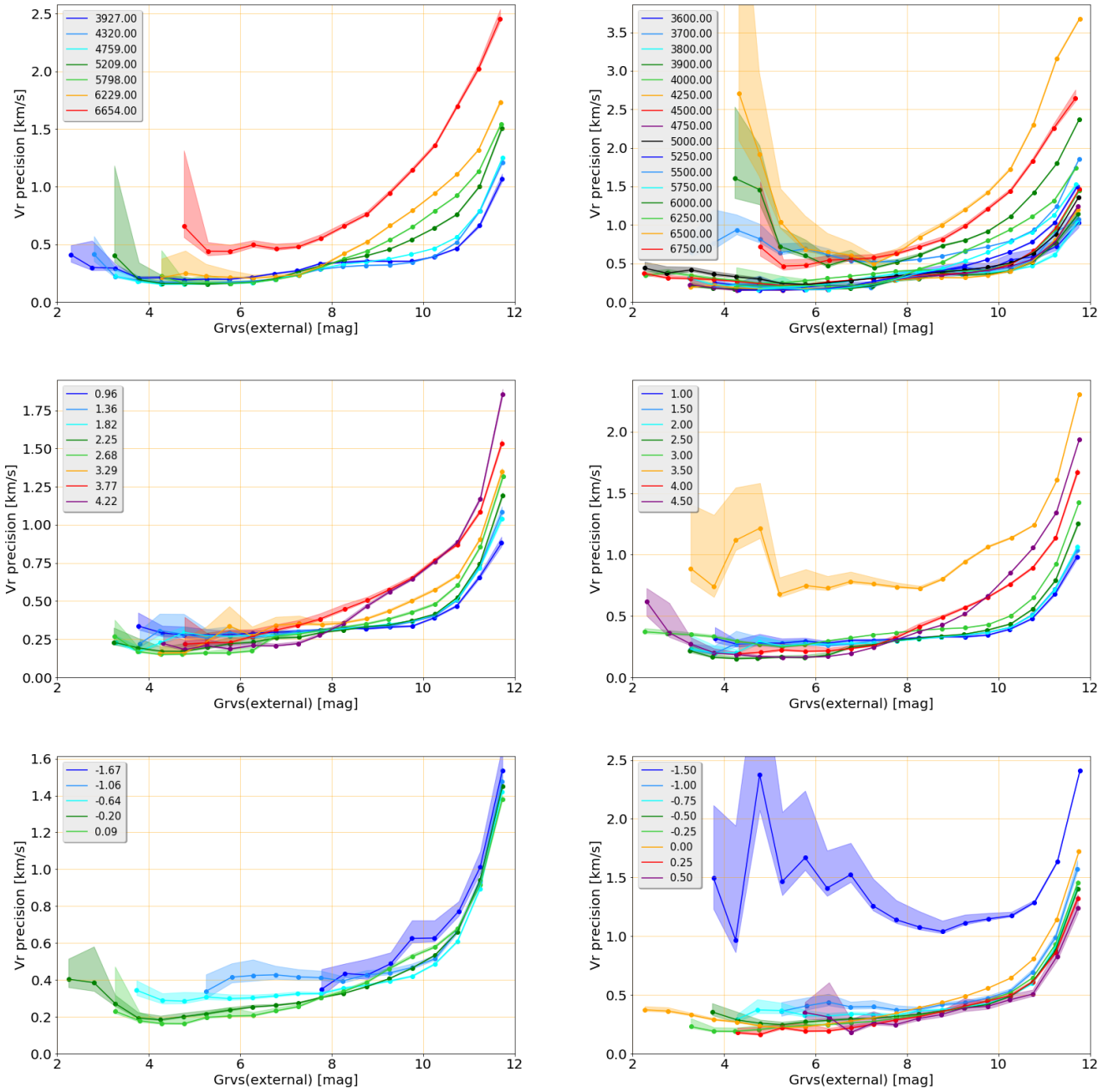

Fig. 19: Top left: Radial velocity precision as a function of $G_{\rm RVS}^{\rm ext}$ magnitude and effective temperature. Each curve corresponds to an interval of 500 K: e.g. [3500, 4000] K (dark blue), [4000, 4500] K (blue). The mean effective temperature of each interval is given in the legend. Top right: Radial velocity precision as a function of $G_{\rm RVS}^{\rm ext}$ magnitude and template effective temperature. Each curve corresponds to the effective temperature of a node in the grid of templates used by the spectroscopic pipeline to derive the radial velocities. The effective temperatures of the nodes are given in the legend. Middle left: Radial velocity precision as a function of $G_{\rm RVS}^{\rm ext}$ magnitude and surface gravity. Each curve corresponds to an interval of 0.5 in surface gravity: e.g. [0.5, 1.0] (dark blue), [1.0, 1.5] (blue). The mean surface gravity of each interval is given in the legend. Middle right: Radial velocity precision as a function of $G_{\rm RVS}^{\rm ext}$ magnitude and template surface gravity. Each curve corresponds to the surface gravity of a node in the grid of templates used by the spectroscopic pipeline to derive the radial velocities. The surface gravities of the nodes are given in the legend. Bottom left: Radial velocity precision as a function of $G_{\rm RVS}^{\rm ext}$ magnitude and metallicity. Each curve corresponds to an interval of 0.5 dex: e.g. [-2.0, -1.5] dex (dark blue), [-1.5, -1.0] dex (blue). The mean metallicity of each interval is given in the legend. Bottom right: Radial velocity precision as a function of $G_{\rm RVS}^{\rm ext}$ magnitude and template metallicity. Each curve corresponds to the metallicity of a node in the grid of templates used by the spectroscopic pipeline to derive the radial velocities. The metallicities of the nodes are given in the legend. The lower and upper 1-σ uncertainties on the measures of the precision are represented as shaded areas.

than those included in the ground-based compilation, which explains the swapping of some curves. At $G_{\rm RVS}^{\rm ext}$ = 11.75 mag, the precision is $\sim$ 3.7 km s^{-1} at $T_{\rm eff}^{\rm tpl} \sim$ 6500 K, $\sim$ 2.6 km s^{-1} at $T_{\rm eff}^{\rm tpl} \sim$ 6750 K, $\sim$ 1.5 km s^{-1} at $T_{\rm eff}^{\rm tpl} \sim$ 5750 K, $\sim$ 1.4 km s^{-1} at $T_{\rm eff}^{\rm tpl} \sim$ 5000 K and $\sim$ 1.1 km s^{-1} at $T_{\rm eff}^{\rm tpl} \sim$ 3900 K.

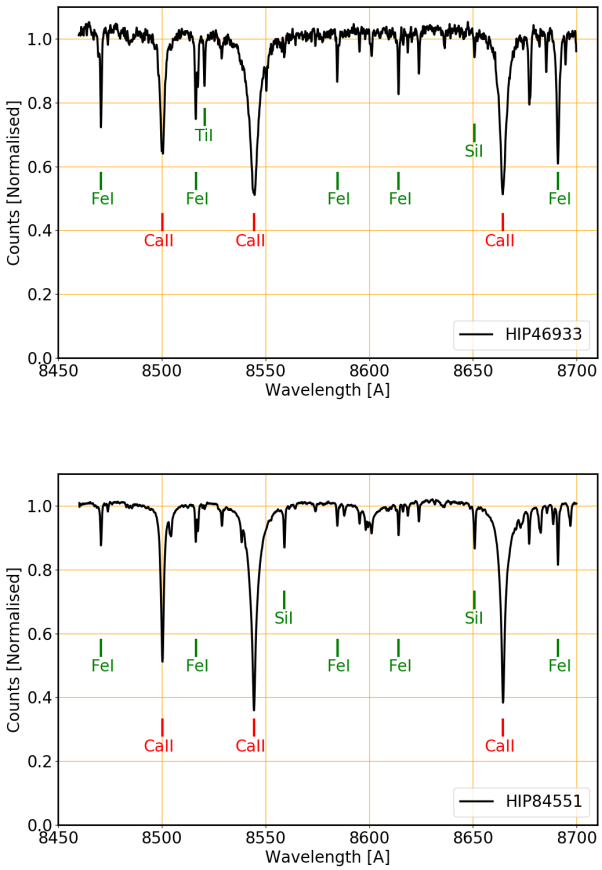

Fig. 20: Comparison of the RVS spectra of HIP46933 and HIP84551. The weak neutral lines are on average stronger in the former which is cooler, $T_{\rm eff}$ = 4487 K, than in the latter, $T_{\rm eff}$ = 6517 K and therefore allow us to derive higher precision radial velocities (at similar $G_{\rm RVS}$ magnitude).

The precision as a function of effective temperature (Fig. 19 top left) is representative of the performance achieved for the 1.3 million stars with known ground-based effective temperature and therefore with the smallest template mismatches. The precision as a function of the template effective temperature (Fig. 19 top right) is representative of the full 7.2 million *Gaia* DR2 stars and account for the full variety of template mismatches. The faint stars precisions as a function of magnitude and effective temperatures quoted in the abstract and conclusion are therefore those estimated using the full sample split by template effective temperature range, which are more representative of the *Gaia* DR2 radial velocities as a whole.

5.3.5. Precision versus magnitude and surface gravity

As shown in the middle row of Figure 19, overall, at the faint end, the radial velocity precision improves as the stellar and template surface gravities decrease. Stars processed with a template with surface gravity $\log g$ = 3.5 show worse performance. This is the consequence of a larger mismatch between the templates and the observed RVS spectra. In the reduced library used by the software module *determineAP*, there is a single synthetic spectra with $T_{\rm eff}^{\rm tpl}$ = 6000 and a single one with 6500 K, both having a surface gravity of 3.5. The restricted library also contains 2 solar metallicity templates with an effective temperature of 5500 K and surface gravities of 3.5 and 4.5. As discussed in Sect. 5.3.4, stars processed with templates selected in the restricted library of 28 synthetic spectra, usually suffer from a larger template mismatch (and therefore worse radial velocity precision) than the stars with stellar parameters contained in the ground-based compilation.

5.3.6. Precision versus magnitude and metallicity

Figure 19 (bottom left) presents the radial velocity precision as a function of the external $G_{\rm RVS}^{\rm ext}$ magnitude and metallicity (the different curves), estimated using the full dataset. As expected, as the metallicity increases, the metallic lines get stronger and the radial velocity precision improves. Yet, over the metallicity range probed in Fig. 19 (bottom left), i.e. $\sim [-2.0, 0.5]$ dex, the precision is only weakly sensitive to metallicity (e.g. compared to the sensitivity to temperature). The limited number of very metal-poor stars, with known metallicities in our compilation of ground-based catalogues, prevents to assess a reliable precision below [Fe/H] = −2 dex. Figure 21 shows the individual radial velocity residuals of the CU6GB, SIM, RAVE, APOGEE and GES validation stars. Stars more metal-poor than −2 dex mostly show (absolute) residuals smaller than 4 km s^{-1}. Figure 22 shows the RVS spectrum of the metal-poor star HD 122563: $T_{\rm eff}$ = 4608 K, $\log g$ = 1.61, [Fe/H] = −2.64 dex (Jofré et al. 2014). Even at this very low metallicity, the ionised calcium lines are still well visible and allow to derive precise radial velocities.

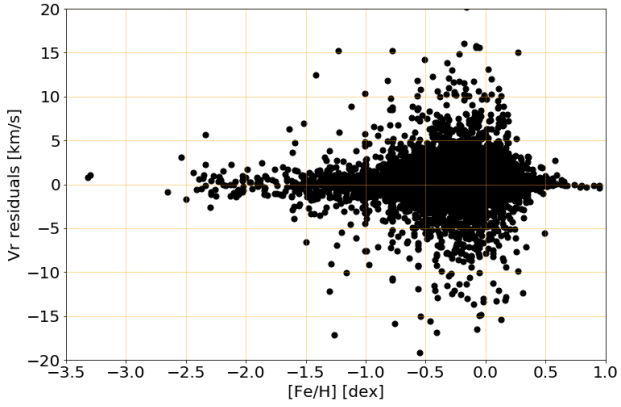

Fig. 21: Radial velocity residuals versus metallicity for the CU6GB, SIM, RAVE, APOGEE and GES validation stars.

Figure 19 (bottom right) presents the radial velocity precision as a function of the external $G_{\rm RVS}^{\rm ext}$ magnitude and metallicity of the template (the different curves), estimated with the full dataset. The reduced library of synthetic spectra used by the software module *determineAP* has two metallicities: −1.5 dex and solar. The stars processed with these two templates suffer, on average, from a stronger template mismatch than the stars processed with the other templates, which have been selected using the parameters from the compilation of ground-based catalogues. As a consequence, stars processed with -1.5 dex or solar metallicity templates show worse performance.

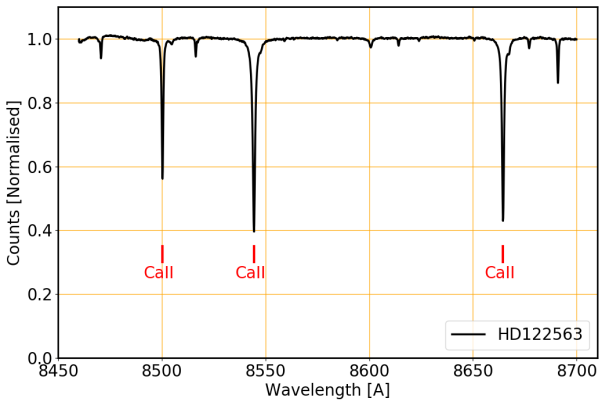

Fig. 22: RVS spectrum of the metal-poor star HD 122563, of metallicity [Fe/H] = −2.64 dex (Jofré et al. 2014). At this metallicity, the ionised calcium triplet is still well visible.

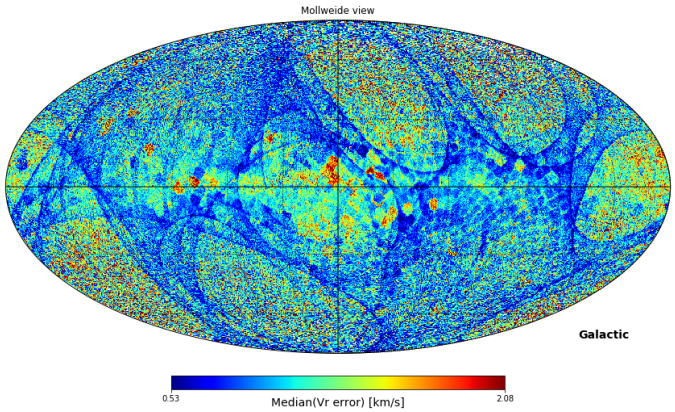

Fig. 23: Map of the radial velocity precision in galactic coordinates. The Galactic Centre is in the middle of the figure and the galactic longitudes increase to the left. The pixel size is 0.2 square degree (healpix level 7).

5.3.7. Template selection in future *Gaia* releases

In *Gaia* DR2, the 280 million spectra to process, the available processing power and the tight processing schedule have imposed a limit of 28 spectra to the library of templates used by the software module *determineAP*. In the subsequent *Gaia* releases, the elaborated analysis of Bp, Rp and RVS spectra (for the brightest stars) should provide precise atmospheric parameters for most *RVS* stars (Bailer-Jones et al. 2013; Recio-Blanco et al. 2016). The spectroscopic pipeline will rely less and less on the module *determineAP* and its limited choice of templates. An increasing fraction of the templates will be selected in the full library of 5256 synthetic spectra using *Gaia* DR3 and *Gaia* DR4 atmospheric parameters. This will reduce the mismatch between templates and observed spectra and will improve the radial velocity performance.

5.3.8. Precision versus sky coordinates

Figure 23 presents the sky map, in galactic coordinates, of the radial velocity precision estimated with the full datatset, for pixels of 0.2 square degree. The 2nd and 98th percentiles of the distribution are 0.53 and 2.08 km s^{-1}, while the minimum and maximum are 0.18 and 9.54 km s^{-1}. Comparison with Fig. 9 (bottom) shows that the best precisions are obtained in the area repeatedly scanned by the satellite and where the number of transits is high.

5.3.9. Open clusters

Open clusters are essential targets to evaluate both the consistency of radial velocities among members and the *RVS* zero point by comparison to the literature. The Hyades and Pleaides are particularly well suited for that purpose because they have nearly 200 members each having a *Gaia* DR2 radial velocity, and they have also been well studied with high-resolution spectroscopy. The radial velocity distribution of the astrometric members (Gaia Collaboration et al. 2018a) as a function of G magnitude (Fig. 24) shows a high consistency of the radial velocities on a wide magnitude range, with only the dispersion increasing at faint magnitude. The mean radial velocities of the Hyades and Pleiades are respectively 39.9 ± 0.05 and 5.55 ± 0.10 km s^{-1}, with a standard deviation of ∼ 2 km s^{-1}, according to Gaia Collaboration et al. (2018a), to be compared to 39.29 ± 0.25 and 5.94 ± 0.08 km s^{-1} reported by Mermilliod et al. (2009).

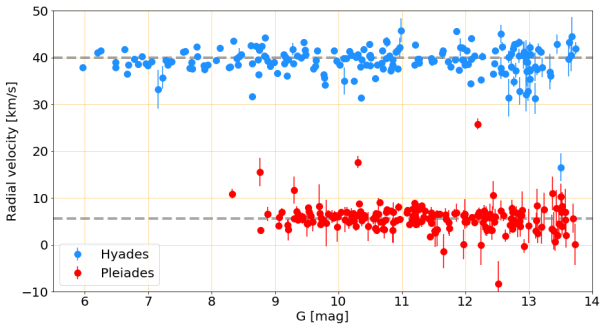

Fig. 24: The figure shows *Gaia* radial velocities for the astrometric members of the Hyades and Pleiades provided by Gaia Collaboration et al. (2018a) as a result of their membership analysis of nearby open clusters. There are nearly 200 stars in each of these two clusters having a Gaia radial velocity. The grey lines indicate the weighted averages of the radial velocity resulting from the analysis performed by Gaia Collaboration et al. (2018a). The dispersion around the mean is ∼2 km s^{-1}.

Other open clusters can be used for comparison to the literature, based on astrometric membership established by Gaia Collaboration et al. (2018a) and Arenou et al. (2018). The weighted mean radial velocity has been determined for open clusters having at least four *Gaia* DR2 member stars with a good radial velocity measurement (i.e. uncertainty smaller than 5 km s^{-1}) after rejection of outliers deviating by more than 10 km s^{-1} from the median cluster velocity. Comparison is made with radial velocities compiled in the catalogue of Dias et al. (2002) updated in 2016, excluding the clusters whose ground-based radial velocities were derived from 1 or 2 stars only, as well as the cluster NGC 6991 which is flagged *"n", i.e. "non-existent NGC"*, in Dias et al. (2002). The difference of radial velocity is shown in Fig. 25 for 63 clusters in common. Three clusters show RV differences larger than 5 km s^{-1}. For NGC 2422 and Trumpler 10, the *Gaia* DR2 radial velocities differ by ∼10 km s^{-1} from Dias' values. However both clusters have also been studied with RAVE by Conrad et al. (2017) who determined mean radial velocities in good agreement with that from *Gaia* DR2 in the two

cases. Stock 12 has the largest radial velocity difference between Gaia and Dias with 14.3 ± 4.2km s^{-1} based on 10 stars on the *Gaia* DR2 side and 4 stars in Dias catalogue. No other determination exists in the literature. For the other clusters the agreement of the *Gaia* DR2 radial velocities and that of the literature is good with a median difference of 0.4 km s^{-1} and a standard deviation of 1.1 km s^{-1}.

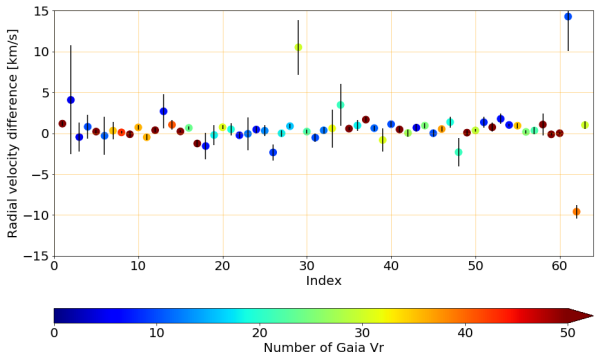

Fig. 25: Difference of mean radial velocities between *Gaia* and the literature (Dias et al. 2002) for 63 open clusters. The error bars correspond to the quadratic sum of *Gaia* and literature uncertainties. The abscissa is an arbitrary number of the clusters from 1 to 63. The colour code highlights the number of *Gaia* members per cluster, which varies from 5 to 191.

6. Conclusion

Gaia DR2 contains median radial velocities for 7 224 631 stars brighter than $G_{\rm RVS} = 12$ mag and with effective temperatures in the range [3550, 6900] K. These stars offer a full sky coverage and a completeness with respect to the full second *Gaia* data release of 77.2%, for stars with $G \leq 12.5$ mag. The accuracy of the radial velocities has been assessed by comparison to several ground-based catalogues. The medians of the radial velocity residuals vary from one catalogue to another, but do not exceed a few 100s m s^{-1}. In addition, *Gaia* DR2 radial velocities present a positive trend with magnitude, starting around $G_{\rm RVS} = 9$ mag and rising up to ~ 500 m s^{-1} at $G_{\rm RVS} = 11.75$ mag. The origin of the trend is under investigation, with the aim to correct for it in *Gaia* DR3. The radial velocity precision has been assessed both by comparison with ground-based catalogues and using the distribution of *Gaia* radial velocity uncertainties. For bright stars with $G_{\rm RVS}$ in [4, 8] mag, the radial velocity precision, estimated using the full dataset, is in the range 220-350 m s^{-1}. At the faint end, $G_{\rm RVS} = 11.75$ mag, the precisions are respectively 1.4 and 3.7 km s^{-1} for $T_{\rm eff} = 5000$ and 6500 K.

Beyond *Gaia* DR2 several data releases are already planned[6]. Each one should include refined data treatments, new functionalities, new products and for the radial velocities a fainter processing limit. *Gaia* DR3 should include radial velocities for stars down to $G_{\rm RVS} = 14$ mag, while *Gaia* DR4 aims at reaching the limiting magnitude of the *Radial Velocity Spectrometer*: $G_{\rm RVS} = 16.2$ mag.

Acknowledgements. This work has made use of results from the European Space Agency (ESA) space mission *Gaia*, the data from which were processed by the *Gaia* Data Processing and Analysis Consortium (DPAC). Funding for the DPAC has been provided by national institutions, in particular the institutions participating in the *Gaia* Multilateral Agreement. The *Gaia* mission website is `http://www.cosmos.esa.int/gaia`. Most of the authors are current or past members of the ESA *Gaia* mission team and of the *Gaia* DPAC and their work has been supported by the French Centre National de la Recherche Scientifique (CNRS), the Centre National d'Etudes Spatiales (CNES), the Agence Nationale de la Recherche, the Région Aquitaine, the Université de Bordeaux, the Utinam Institute of the Université de Franche-Comté, and the Institut des Sciences de l' Univers (INSU); the Science and Technology Facilities Council and the United Kingdom Space Agency; the Belgian Federal Science Policy Office (BELSPO) through various Programme de Développement d'Expériences Scientifiques (PRODEX) grants; the German Aerospace Agency (Deutsches Zentrum fur Luft- und Raumfahrt e.V., DLR); the Algerian Centre de Recherche en Astronomie, Astrophysique et Géophysique of Bouzareah Observatory; the Swiss State Secretariat for Education, Research, and Innovation through the ESA PRODEX programme, the Mesures d'Accompagnement, the Swiss Activités Nationales Complémentaires, and the Swiss National Science Foundation; the Slovenian Research Agency (research core funding No. P1-0188). This research has made use of the SIMBAD database (Wenger et al. 2000) developed and operated at CDS, Strasbourg, France.

[6] `https://www.cosmos.esa.int/web/gaia/release`

References

Abolfathi, B., Aguado, D. S., Aguilar, G., et al. 2017, ArXiv e-prints [arXiv:1707.09322]
Adibekyan, V. Z., Sousa, S. G., Santos, N. C., et al. 2012, A&A, 545, A32
Anderson, E. & Francis, C. 2012, Astronomy Letters, 38, 331
Andrae, R., Fouesneau, M., Creevey, O., et al. 2018, A&A (special issue for Gaia DR2)
Arenou, F., Luri, X., Babusiaux, C., et al. 2018, A&A (special issue for Gaia DR2)
Bailer-Jones, C. A. L., Andrae, R., Arcay, B., et al. 2013, A&A, 559, A74
Baranne, A., Queloz, D., Mayor, M., et al. 1996, A&AS, 119, 373
Buder, S., Asplund, M., Duong, L., et al. 2018, MNRAS, 478, 4513
Conrad, C., Scholz, R. D., Kharchenko, N. V., et al. 2017, A&A, 600, A106
Cropper, M., Katz, D., Sartoretti, P., et al. 2018, A&A (special issue for Gaia DR2)
Cui, X.-Q., Zhao, Y.-H., Chu, Y.-Q., et al. 2012, Research in Astronomy and Astrophysics, 12, 1197
Dias, W. S., Alessi, B. S., Moitinho, A., & Lépine, J. R. D. 2002, A&A, 389, 871
Evans, D., Riello, M., De Angeli, F., et al. 2018, A&A (special issue for Gaia DR2)
Gaia Collaboration, Babusiaux, C., van Leeuwen, F., et al. 2018a, A&A (special issue for Gaia DR2)
Gaia Collaboration, Brown, A., Vallenari, A., et al. 2018b, A&A (special issue for Gaia DR2)
Gaia Collaboration, Brown, A. G. A., Vallenari, A., et al. 2016a, A&A, 595, A2
Gaia Collaboration, Prusti, T., de Bruijne, J. H. J., et al. 2016b, A&A, 595, A1
Gilmore, G., Randich, S., Asplund, M., et al. 2012, The Messenger, 147, 25
Holtzman, J. A., Shetrone, M., Johnson, J. A., et al. 2015, AJ, 150, 148
Houk, N. & Cowley, A. P. 1975, University of Michigan Catalogue of two-dimensional spectral types for the HD stars. Volume I. Declinations -90_ to -53.
Jackson, R. J., Jeffries, R. D., Lewis, J., et al. 2015, A&A, 580, A75
Jofré, P., Heiter, U., Soubiran, C., et al. 2014, A&A, 564, A133
Jordi, C., Gebran, M., Carrasco, J. M., et al. 2010, A&A, 523, A48
Kordopatis, G., Gilmore, G., Steinmetz, M., et al. 2013, AJ, 146, 134
Kos, J., Lin, J., Zwitter, T., et al. 2017, MNRAS, 464, 1259
Kunder, A., Kordopatis, G., Steinmetz, M., et al. 2017, AJ, 153, 75
Lindegren, L., Hernández, J., Bombrun, A., et al. 2018, A&A (special issue for Gaia DR2)
Majewski, S. R., Schiavon, R. P., Frinchaboy, P. M., et al. 2017, AJ, 154, 94
Makarov, V. V. & Unwin, S. C. 2015, MNRAS, 446, 2055
Martell, S. L., Sharma, S., Buder, S., et al. 2017, MNRAS, 465, 3203
Mayor, M., Pepe, F., Queloz, D., et al. 2003, The Messenger, 114, 20
Mermilliod, J.-C., Mayor, M., & Udry, S. 2009, A&A, 498, 949
Nordström, B., Mayor, M., Andersen, J., et al. 2004, A&A, 418, 989
Perruchot, S., Kohler, D., Bouchy, F., et al. 2008, in Proc. SPIE, Vol. 7014, Ground-based and Airborne Instrumentation for Astronomy II, 70140J
Queloz, D., Mayor, M., Udry, S., et al. 2001, The Messenger, 105, 1
Recio-Blanco, A., de Laverny, P., Allende Prieto, C., et al. 2016, A&A, 585, A93
Reid, M. J., Menten, K. M., Brunthaler, A., et al. 2014, ApJ, 783, 130
Riello, M., De Angeli, F., Evans, D., et al. 2018, A&A (special issue for Gaia DR2)
Sacco, G. G., Morbidelli, L., Franciosini, E., et al. 2014, A&A, 565, A113

Sartoretti, P., Katz, D., Cropper, M., et al. 2018, A&A (special issue for Gaia DR2)
Soubiran, C., Jasniewicz, G., Chemin, L., et al. 2018, A&A (special issue for Gaia DR2)
Steinmetz, M., Zwitter, T., Siebert, A., et al. 2006, AJ, 132, 1645
Wenger, M., Ochsenbein, F., Egret, D., et al. 2000, A&AS, 143, 9
Yanny, B., Rockosi, C., Newberg, H. J., et al. 2009, AJ, 137, 4377
Zhao, G., Zhao, Y.-H., Chu, Y.-Q., Jing, Y.-P., & Deng, L.-C. 2012, Research in Astronomy and Astrophysics, 12, 723
Zwitter, T., Kos, J., Chiavassa, A., et al. 2018, ArXiv e-prints [arXiv:1804.06344]

[1] GEPI, Observatoire de Paris, Université PSL, CNRS, 5 Place Jules Janssen, 92190 Meudon, France
[2] Mullard Space Science Laboratory, University College London, Holmbury St Mary, Dorking, Surrey RH5 6NT, United Kingdom
[3] Royal Observatory of Belgium, Ringlaan 3, 1180 Brussels, Belgium
[4] Laboratoire Univers et Particules de Montpellier, Université Montpellier, CNRS, Place Eugène Bataillon, CC72, 34095 Montpellier Cedex 05, France
[5] CNES Centre Spatial de Toulouse, 18 avenue Edouard Belin, 31401 Toulouse Cedex 9, France
[6] CRAAG - Centre de Recherche en Astronomie, Astrophysique et Géophysique, Route de l'Observatoire Bp 63 Bouzareah 16340, Alger, Algérie
[7] Institut d'Astrophysique et de Géophysique, Université de Liège, 19c, Allée du 6 Août, B-4000 Liège, Belgium
[8] Universiteit Antwerpen, Onderzoeksgroep Toegepaste Wiskunde, Middelheimlaan 1, 2020 Antwerpen, Belgium
[9] F.R.S.-FNRS, Rue d'Egmont 5, 1000 Brussels, Belgium
[10] Thales Services for CNES Centre Spatial de Toulouse, 18 avenue Edouard Belin, 31401 Toulouse Cedex 9, France
[11] Department of Astronomy, University of Geneva, Chemin d'Ecogia 16, CH-1290 Versoix, Switzerland
[12] Leibniz Institute for Astrophysics Potsdam (AIP), An der Sternwarte 16, 14482 Potsdam, Germany
[13] Laboratoire d'astrophysique de Bordeaux, Université de Bordeaux, CNRS, B18N, allée Geoffroy Saint-Hilaire, 33615 Pessac, France
[14] Laboratoire Lagrange, Université Nice Sophia-Antipolis, Observatoire de la Côte d'Azur, CNRS, CS 34229, F-06304 Nice Cedex, France
[15] Instituto de Astrofísica de Canarias, E-38205 La Laguna, Tenerife, Spain
[16] Universidad de La Laguna, Departamento de Astrofísica, E-38206 La Laguna, Tenerife, Spain
[17] Univ. Grenoble Alpes, CNRS, IPAG, 38000 Grenoble, France
[18] Max Plank Institute für Sonnensystemforschung, Justus-von-Liebig-Weg 3, D-37077 Göttingen, Germany
[19] Unidad de Astronomía, Fac. Cs. Básicas, Universidad de Antofagasta, Avda. U. de Antofagasta 02800, Antofagasta, Chile
[20] ATOS for CNES Centre Spatial de Toulouse, 18 avenue Edouard Belin, 31401 Toulouse Cedex 9, France
[21] Max Planck Institute for Extraterrestrial Physics, High Energy Group, Gießenbachstraße, 85741 Garching, Germany
[22] Institute for Astronomy, University of Edinburgh, Royal Observatory, Blackford Hill, Edinburgh EH9 3HJ, United Kingdom
[23] LNE-SYRTE, Observatoire de Paris, Université PSL, CNRS, Sorbonne Université, 61 avenue de l'Observatoire 75014 Paris
[24] Faculty of Mathematics and Physics, University of Ljubljana, Jadranska ulica 19, 1000 Ljubljana, Slovenia
[25] INAF-Osservatorio Astronomico di Padova, vicolo Osservatorio 5, 35122 Padova, Italy
[26] INAF Astronomical Observatory of Padova, I-36012 Asiago (VI), Italy
[27] Research School of Astronomy and Astrophysics, Australian National University, Canberra, ACT 2611, Australia

Appendix A: Distribution of the template parameters

Figures A.1 show the distributions of the effective temperatures (top), surface gravities (middle) and metallicities (bottom) of the templates. The alternation of tall and small peaks in the effective temperature distribution is the consequence of certain temperatures being chosen only when the stars are contained in the ground based catalogue compilations (producing small peaks). Similar selection effects are visible for surface gravity (few templates with $\log g \leq 2.5$ or equal to 4) and metallicity (templates mostly solar, with a *"small"* secondary peak at [Fe/H] = −1.5 dex, which are the metallicities in the sub-library used by the dedicated selection module).

Appendix B: Charge Transfer Inefficiency

As described in Sect. 5.2.2, the *Gaia* radial velocities exhibit a trend with magnitude. The first lead explored to explain this trend was the Charge Transfer Inefficiency (CTI). When they hit the CCDs, high energy particles damage the pixels, producing traps which could snare a fraction of the spectrum photo-electrons, preventing them to be propagated consistently with the rest of the signal from CCD column to CCD column. Eventually, the trapped photo-electrons are released. If the release time is short (i.e. the time for the spectrum to be propagated by one or a few pixels), the CTI does not remove signal from the spectrum, but instead distorts the Line Spread Function (LSF) profile, producing a trail in the direction opposite to the propagation of the spectrum. In the RVS, the blue edge of the spectrum is leading. The CTI would therefore produce a tail on the LSF red edge, shifting the line centroids to higher wavelengths and applying a positive shift to the radial velocities. Pre-launch ground-based laboratory tests have shown that the impact of CTI increases as the signal decreases. We would therefore expect from CTI a positive radial velocity trend with magnitude, which is what we observe. The CTI effect is also expected to increase with time, as the radiation damages accumulate. This prediction is not verified by the *Gaia* radial velocities. The trend appears stable in time. The CTI is therefore unlikely to be causing the trend.

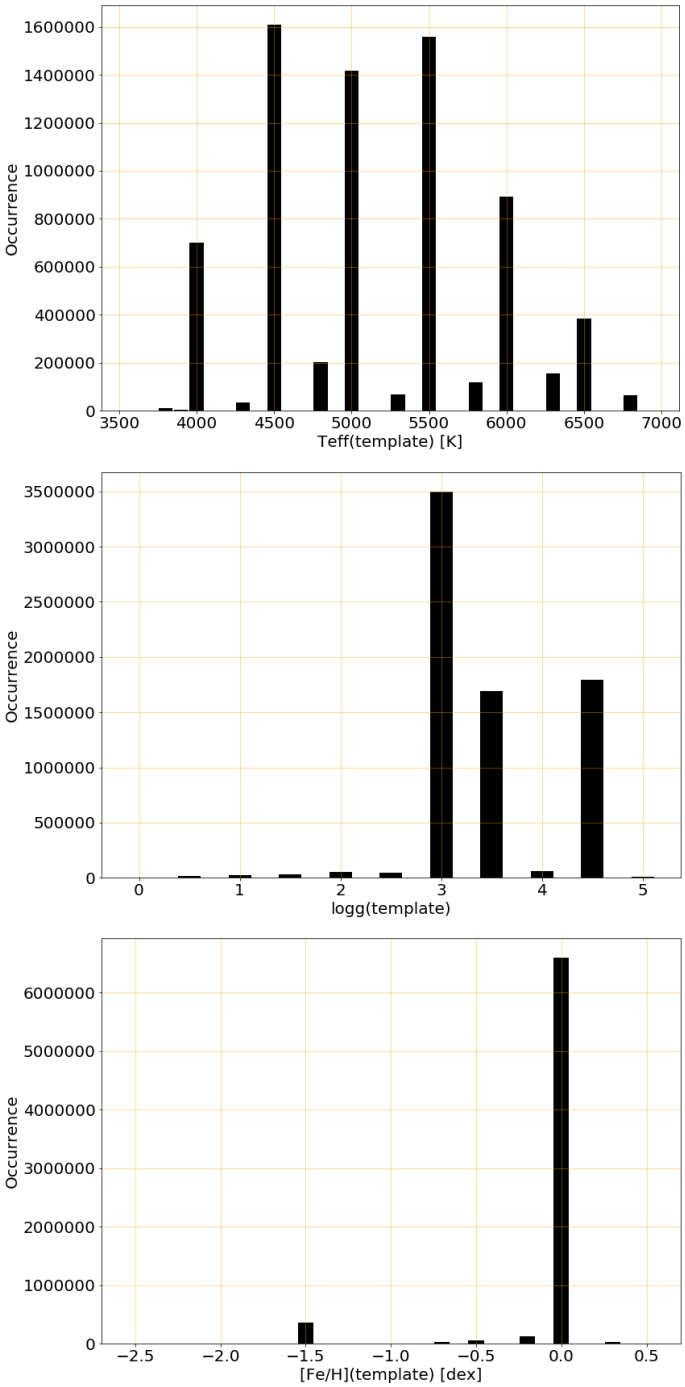

Fig. A.1: Top: Distribution of the effective temperatures of the templates. Middle: Distribution of the surface gravities of the templates. Bottom: Distribution of the metallicities of the templates.